universität wien

MASTERARBEIT / MASTER'S THESIS

Titel der Masterarbeit / Title of the Master's Thesis

„Variation of the *N*-donor moiety of tridentate *N,O,O*–naphthoquinone complexes"

verfasst von / submitted by

Paul Thrakl, BSc

angestrebter akademischer Grad / in partial fulfilment of the requirements for the degree of

Master of Science (MSc)

Wien, 2024 / Vienna 2024

Studienkennzahl lt. Studienblatt / degree programme code as it appears on the student record sheet:	A 066 862
Studienrichtung lt. Studienblatt / degree programme as it appears on the student record sheet:	Masterstudium Chemie
Betreut von / Supervisor:	o. Univ.–Prof. Dr. Dr. Bernhard Keppler
Mitbetreut von / Co-Supervisor:	DI Dr. Wolfgang Kandioller

Acknowledgements

I would like to express my gratitude to my supervisor o. Univ.–Prof Dr. Dr. Bernhard Keppler for giving me the opportunity to work in the fascinating field of bioinorganic chemistry.

Additionally, I would also like to offer my sincere gratitude to my co–supervisor Dipl.–Ing. Dr. Wolfgang Kandioller for always finding time for a meeting and ensuring that no question is left unanswered.

My appreciation also goes to the NMR and MS team of the University of Vienna for measuring all my samples, as well as Mag. Theiner and the microanalytical laboratory team for conducting the elemental analysis of my samples.

I extend my thanks to my colleagues Alex, Paul, Florian, Julie, and Andreas for always providing valuable advice, assisting me in finding solutions to any problems that I encountered and for keeping me excellent company during my practical work.

Furthermore, I would like to thank all members of the faculty of inorganic chemistry for their support.

Special thanks to my parents Christine and Paul as well as my sister, Anna, for supporting me emotionally and financially throughout my whole life while still giving me enough free space for my personal growth. I would also like to thank my girlfriend Jessica who accompanied me during my entire study. Her input on various topics helped me immensely, no matter how "subject-specific" or related to my life choices.

Last but not least, I would like to thank all my friends that I met during my attendance at the University of Vienna.

Abstract

Transition metal-based drugs have established themselves as a cornerstone for many therapies due to their various pharmaceutical properties (e.g., antimicrobial, antiparasitic, antiviral and anticancer). Previous research on organometallic ruthenium(II) arene complexes as potential anticancer drug candidates has led to the discovery of compounds containing an *in-situ* generated tridentate scaffold. This novel class of complexes exhibit remarkable cytotoxic properties due to their outstanding stability in aqueous media while also demonstrating high selectivity in 2D and 3D cell cultures. However, further research is still necessary to fully optimise their capabilities and understand their unique modes of action.

The main purpose of this thesis was to investigate *N*–donor variations of the tridentate naphthoquinone-based *N,O,O*–coordination motif. Various classes of ligands containing a hydrazone moiety were examined for their complexation behaviour, and their respective complexes were synthesized and characterised via NMR spectroscopy and elemental analysis. Eight of these compounds are presented within this work. The most interesting finding from this study is that the *N*-donor moiety may be extended to non-cyclic 1,2–diazole ligands, yet the purification of these novel complexes was not feasible within the scope of this work.

Zusammenfassung

Übergangsmetallbasierte Medikamente haben sich aufgrund ihrer vielfältigen pharmazeutischen Eigenschaften (z. B. antimikrobielle, antiparasitäre, antivirale und antikanzerogenen Aktivitäten) als Eckpfeiler für viele Therapien etabliert. Vorausgegangene Forschung zu organometallischen Ruthenium(II)-Aren-Komplexen als potenzielle Wirkstoffkandidaten gegen Krebs führte zur Entdeckung von Verbindungen, die ein *in-situ* erzeugtes dreizähniges Ligandenmotiv enthalten. Diese neuartige Klasse von Komplexen zeigt bemerkenswerte zytotoxische Eigenschaften aufgrund ihrer herausragenden Stabilität in wässrigen Medien und demonstriert darüber hinaus eine hohe Selektivität in 2D und 3D Zellkulturen. Dennoch ist weitere Forschung erforderlich, um ihre therapeutischen Eigenschaften zu optimieren und ihren einzigartigen Wirkungsmechanismus zu verstehen.

Das Hauptziel dieser Arbeit bestand darin, die Variation des *N*–Donor der dreizähnigen Naphthochinon–basierten *N,O,O*–Koordinationsmotiv zu untersuchen. Für diesen Zweck wurden verschiedene Liganden mit einem Hydrazon Motiv bezüglich ihres Komplexierungsverhalten untersucht und deren entsprechenden Komplexe synthetisiert und mittels NMR-Spektroskopie und Elementaranalyse charakterisiert. Acht dieser Verbindungen werden innerhalb dieser Arbeit vorgestellt.

Die wohl relevanteste Erkenntnis aus dieser Studie ist, dass die *N*–Donor–Einheit auf nichtzyklische 1,2–Diazol Liganden erweitert werden kann, jedoch stellte sich die Aufreinigung dieser neuartigen Komplexe im Rahmen dieser Arbeit als nicht durchführbar heraus.

Content

1. Introduction:

1.1. Cancer

Cancer is a collective term for a group of over 100 different diseases which are originally caused by alterations in the DNA sequence. Cancer can occur in almost any organ or tissue.[1] Despite extensive research in the last few decades leading to a better understanding of these diseases, the treatment of cancer remains an exceptionally complex process.[2]

The adult human body consists of approximately 28–40 trillion cells.[3] In contrast to a single-celled organisms such as bacteria, the cells of an animal are required to collaborate and are willing to self-sacrifice in order to protect the organism from damage. Healthy cell division is heavily regulated through a complex cell cycle control system, involving numerous cycle checkpoint, cell signalling pathways and regulatory mechanisms.

In the course of their lifespan, a significant number of cells experience mutations on a daily basis, which are usually rendered harmless by the cells own repair system. While a single mutation is not sufficient to transform a normal cell into a cancerous one, some mutations can supply the cell with advantages to bypass these important cell regulatory systems. Future clones of the primary mutated cell will follow a process called “clonal evolution”, in which one dominant clone may develop enough selective advantages to outcompete normal and other mutant cells.[4] The accumulation of heritable mutations, which allow abnormal cells to outgrow and outlive their neighbours, can provoke the cell to prioritize its own survival over the general well-being of the whole organism. A group of abnormal cells, usually originating from a single mutated cell, may form a tumour. Tumours are a mass of cell tissue formed by an overabundance of cell growth.[5] It can either be categorised as cancerous (malignant), not cancerous (benign) or precancerous. Although benign tumours remain localized and do not metastasize, their uncontrolled proliferation may still pose a thread by displacing surrounding tissue or organs. Malignant tumours on the other hand are invasive and can travel to other areas of the body through the bloodstream or the lymphatic system (Figure **1**). This process, known as “metastasis”, is attributed as the primary cause of death for over 90% of cancer patient.[6,7] Once these metastatic tumours have inserted themselves into a new viable location, they induce angiogenesis, allowing them to compete with healthy cells and organs for essential nutrition and oxygen to sustain their aggressive metabolic behaviour.

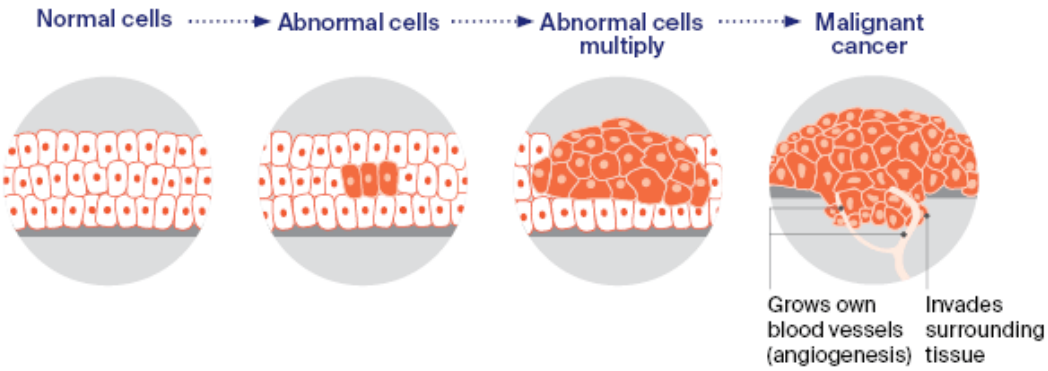

Figure 1: The development of cancer.[7]

Different types of cancer are classified by their side of origin. Each type of cancer has different features, characteristics, and response to treatment, depending on the cells the malignant tumour originated from.[8] For instance, if lung cancer spreads to surrounding lymphocytes, the secondary cancer is still classified as metastatic lung cancer instead of a lymphoma. This poses new challenges in the battle against cancer as individual tumour types may response differently to certain therapies. Therefore, a fundamental understanding of this subject is essential to be able to differentiate between the diverse cancer variations.

1.1.1. The hallmarks of cancer

In 2000, Hanahan and Weinberg proposed the first six hallmarks of cancer (Figure **2**).[9] Each individual hallmark represents a fundamental characteristic with which cancer cells distinguish themselves from normal cells and which may help in understanding the intricate biology of cancer.

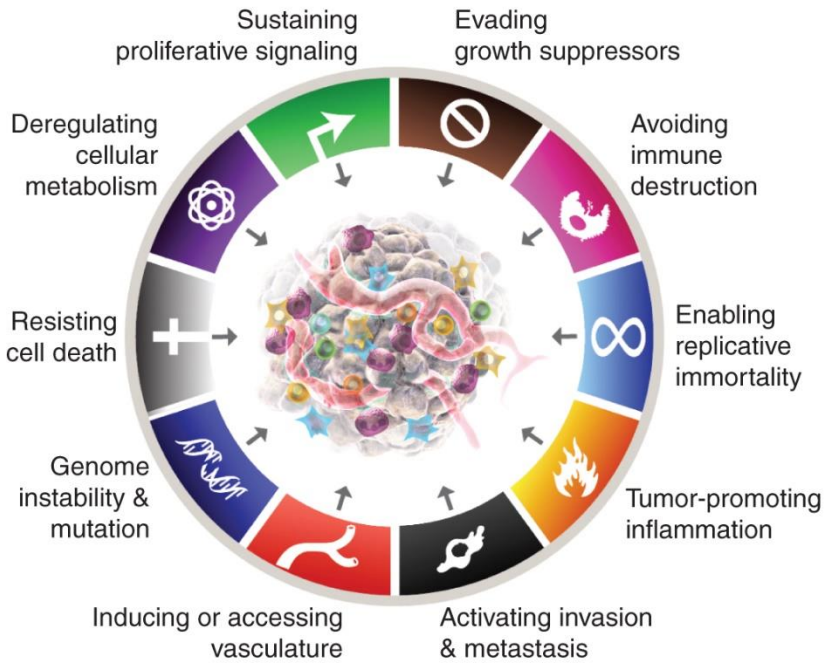

Figure 2:The hallmarks of cancer as proposed by Hanahan and Weinberg in 2011.[10]

The first six hallmarks of cancer proposed in 2000:[9]

Sustaining proliferation signalling

Proliferation of healthy tissue is heavily regulated to preserve the genetic integrity. To initiate the cell division cycle, cells are dependent on extracellular growth factors to bind to corresponding transmembrane tyrosine kinase receptors to stimulate nuclear transcription factors which regulate gene expression.[11] Cancer cells, on the other hand, are not reliant on this normal growth factor signalling pathway and might develop an independency to the feedback of neighbouring cells. By increasing the production of growth-promoting signals or amplifying the sensitivity to growth factors by increasing the levels of receptor proteins displayed at the surface of cells, cancer cells may stimulate their own growth.

Evading growth suppressors

Even though a wide variety of tumour suppressors have been identified, the cell division regulating proteins RB (retinoblastoma-associated) and p53 act as the two fundamental suppressors of the cell division cycle. RB responds to proliferation inhibitory signals from mainly outside of the cell whereas TP53 responds to stress and abnormality inside the cell. When a sensor protein detects DNA damage, p53 binds to a specific DNA sequence, thereby inhibiting cell cycle progression and activating repair proteins. In cases of irreparable damage, p53 may induce apoptosis or senescence.[12,13]

According to a study conducted by Zhang et al in 2016 about the mutation of p53 in ovaria cancer, 50% of all types of cancer in humans, and 97% of all cases of HGSOCs (high grade serous ovarian cancer), the most common and simultaneously aggressive type of ovarian cancer, exhibit a mutation in TP53, the gene encoding for the tumour suppressor protein p53.[14] Compromised function of p53 can lead to unchecked cell proliferation.

Activating invasion and metastasis

Invasion is the process of extension into the surrounding tissue, whereas metastasis involves the establishments of colonies in distant organs which can be reached through the blood circulation or lymphatic system. In the process of tumour progression, cancer cells may undergo a process called EMT (epithelial to mesenchymal transition), transforming the primary immobile epithelial cells into mesenchymal cells.[15] In this state, benign tumour cells lose tight- and adherens junctions responsible for cell-cell adhesion and acquire enhanced migratory and invasive capabilities that enable degradation and subsequent migration through the extracellular matrix into the circulatory system. The harsh condition in the bloodstream pose challenges, and most cancer cells do not survive this journey.[16,6] Cancer cells can migrate either collectively or as single cells. However, clumps of cancer cells have a higher chance to form metastasis colonies. Following their establish in a new environment, cancer cells can revert to epithelial state through the MET (mesenchymal to epithelial transition) process.[17]

Albeit cancer is able to metastasise to various parts of the body, different types of cancer often exhibit preferences for specific metastatic sites based on the origin of the primary tumour. Certain organs, like the lungs, liver or brain provide cancer cells a supportive microenvironment with which they can grow and thrive in. This occurrence was first described by Stephen Paget in 1899 as the “seed and soil” theory.[18,19] “The “Seed and soil” is an appealing metaphor, but it can be misleading. To disseminated cancer cells (seeds), every distant soil (tissue) is deadly, though some soils may be less deadly than others.”[20] Nevertheless, metastasis to less common areas is still possible, depending on the varying degrees of aggressiveness among different types of cancer.

Due to stressful conditions in their new environment, some cancer cells go dormant after their arrival at secondary sites until more favourable conditions are met. This reactivation can happen after a long period of time, even if the primary tumour has long been eradicated.[16]

Enabling replicative immortality

In normal cells linages, the telomeric ends, a repetitive sequence of six nucleotides, are shortened after each cell division cycle. Once the telomeres are too short, the cell experiences a crisis state which leads to cell death to prevent the formation of flawed dicentric chromosomes. This can be prevented by telomerase, a DNA polymerase, which is usually absent in non-immortalized cells. Telomerase activity restores the genomic stability by preserving the telomeric length, enabling an infinite replication potential.[11] According to Hanahan and Weinberg, telomerase is overexpressed in the majority (~90%) of immortalized cells like human cancer cells.[21] Cancer cells can upregulate the telomerase activity by epigenetic or random mutations to preserve the function of the DNA despite their rapid cell division, allowing the tumour to grow and spread.[21,22]

Inducing angiogenesis

To assure the survival of a tumour and to sustain rapid cell growth, mutated cells need a constant supply of oxygen, nutrients, and growth factors. This is accomplished by the formation of new blood vessels through "sprouting" from existing vessels. In an adult human, angiogenesis is mostly limited to precise occurrences like wound healing, the menstrual cycle or muscle growth.[23] To induce the formation of new blood vessels even without an injury of the tissue, cancer cells "flip the angiogenic switch" by suppressing angiogenic inhibitors, like angiostatin and p53, or upregulating inducers like the vesicular endothelial growth factor (VEGF) and fibroblast growth factor.[24] An increased activity of angiogenic inducers can be a biomarker for cancer.[25]

Resisting cell death

As previously discussed, apoptosis is the natural induced self-destroy mechanism of the cells which can either be stimulated by an extrinsic (death receptor-mediated) or an intrinsic (mitochondrial-mediated) pathway.[26] The hallmark "resisting cell death" refers to the acquired resistance to intrinsic apoptosis, initiated from within the cell, rather than apoptosis triggered by external signals.[27]

As depicted in Figure **3**, the intrinsic pathway is induced by the release of the proapoptotic signalling protein cytochrome c from the mitochondria into the cytosol as an answer to stress signals. Together with the proteins procaspase-9 and Apaf-1, cytochrome c forms the apoptosome, a large protein structure, which triggers the caspase-cascade, ultimately resulting in programmed cell death.[2,10,24]

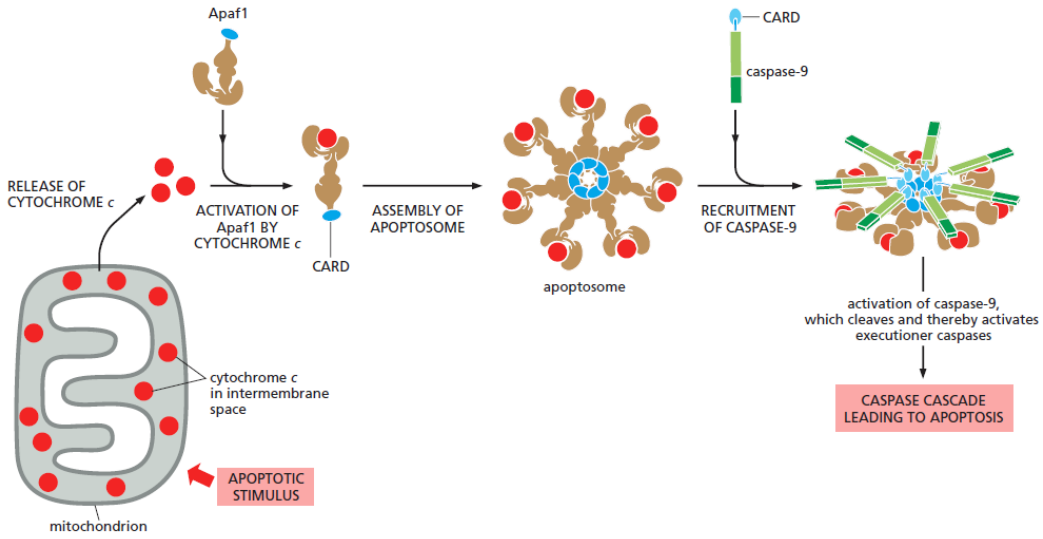

Figure 3:Depiction of the intrinsic signalling pathway.[5]

Proteins of the Bcl-2 family are heavily involved in the regulation of apoptosis, exhibiting either displaying anti- or pro-apoptotic properties. By influencing the expression levels of the various Bcl-2 proteins, cytochrome c or IAP (inhibitors of apoptosis) proteins, cancer cells may resist cell death.[28]

Eleven years later, two more hallmarks and two enabling characteristics were added to the core set.[21] The biggest advance was the better understanding of the invasion and metastasis mechanisms of cancer.

The two additional hallmarks introduced in 2011:

Avoiding immune destruction

The body´s natural defence mechanism is directed to detect and eliminate abnormal cells. Through various mechanisms, cancer may develop the ability to escape recognition and attacks by the hosts immune system. This includes displaying proteins on their surface which bind to inhibitory receptors on the surface of T-cells or downregulating the expression of a tumour antigen that would otherwise trigger immune recognition.[29] The tumours protective microenvironment further contributes to immune evasion by secreting highly immunosuppressive molecules, like regulatory T-cells or myeloid-derived suppressor cells to dampen the effectiveness of a T-cell response.[11]

Tumour-promoting inflammation

The process of inflammation is an innate, protective response of the body to injuries or infections, such as pathogens. Its purpose is to eliminate the cause of cell injury and promote tissue healing.[30] The tumours microenvironment can promote inflammation to recruit immune cells, like macrophages, lymphocytes and neutrophils, forming an inflammatory tumour microenvironment. These inflammatory cells provide cancer cells with growth factors and invasion promoting enzymes.[31] Additionally, tumour cells may secrete chemokines that attract leukocytes to produce cytokines and ROS/NOS (reactive oxygen/nitrogen species). This process may induce genetic mutations and genomic instability, further contributing to the acquisition of malignant traits.[11,32]

The two enabling characteristics of cancer introduced in 2011:

Inducing genome instability and mutations

Compared to normal cell, malignancies often exhibit an increased tendency to form DNA mutations, chromosomal rearrangements, and other genetic abnormalities during cell division due to their deviant proliferation. This genetic instability can be achieved by increasing the rate at which mutations occur by suppressing the genomic maintenance and surveillance machinery. In addition to DNA mutations, epigenetic repression of tumour suppressor genes, like the DNA methylation and histone modification of anti-oncogenes or DNA damage checkpoint genes, play an important role in the development and progression of hereditary cancer.[5,21,33,34]

Deregulating cellular metabolism

Instead of relying on the mitochondrial oxidative phosphorylation, which is the usual pathway for normal cells to process glucose under aerobic conditions, cancer cells often utilize the anaerobic glycolysis to produce lactate as an energy source. Even though the anaerobic glycolysis provides ATP with a much lower efficiency than aerobic oxidative phosphorylation (2 ATP molecules per glucose instead of up to 36 ATP molecules), it allows the cells to generate energy much quicker. The phenomenon that cancer cells use this form of energy production even under aerobic conditions is called the “Warburg effect” after its discoverer, Otto Warburg. It is attributable to the fact, that cancer cells prioritize rapid energy production to supply enough energy for the constant cell growth.[35] Furthermore, some intermediates, which are formed during the glycolysis pathway, can be used to synthesize macromolecules necessary to sustain cell proliferation.[11,24]

In 2022, Hanahan proposed the two more emerging hallmarks “unlocking phenotypic plasticity” and “senescent cells”, as well as the two enabling characteristics “nonmutational epigenetic reprogramming” and “polymorphic microbiomes”, leading to a total of ten hallmarks and four enabling characteristics. However, due to their rather recent addition, they still need to be sufficiently validated.[10]

1.1.2. Cancer in Europe

While cancer is the second-leading cause of death worldwide, it accounts for the highest number of deaths among humans aged under 65 years.[36,37] According to the European Cancer information system (ECIS), new cancer cases rose by 2.3% between 2020 and 2022.[38] Combined, breast, prostate, lung and colorectal cancer represent over half of all cancer cases in Europe.[39] Breast cancer continues to be the most frequently diagnosed cancer, accounting for 13.8% of all cancer diagnoses. The risk of developing cancer in Europe before the age of 75 years is 32.2% for men and 24.8% for woman. Besides the gender disparity in cancer susceptibility, the risk of developing cancer is influenced by other factors like increasing age, unhealthy lifestyle, and poor diet. As life expectancy continues to rise, an increase in cancer incidences is expected in the years to come.[40] Although Europe comprising only a tenth of the world´s population, one in four cancer diagnoses occur within this region. It is important to emphasize that the higher diagnosis rate does not necessarily mean that cancer is more common in Europe, but rather that cancer diseases are more effectively detected and documented due to the general implementation of improved cancer screening programs and diagnostic capabilities in Europe.[40] In addition, the increased live expectancy in developed countries also contributes to the increased number of cancer incidences. Still, despite the recent advances in detection and treatment, 1.96 million people lost their lives to cancer in 2021.[41] The risk of dying from cancer before the age of 75 is estimated at 15% for men and 9% for women.[37] The mortality rate highly depends on the affected body part with the most lethal types of cancer being lung, colorectum, breast and pancreas cancer. While being one of the more preventable type of cancer, lung cancer continues to be the leading cause of cancer-related deaths in men and ranks as the second most prevalent cause among women, following breast cancer. These numbers help to visualise, how prevalent this life-threatening disease is in our society.

1.2. Cancer Therapy

In the beginning of the 19th century, cancer treatment was mostly limited to drastic surgery. Radical mastectomy, pioneered by the American surgeon Halsted, was utilized in the treatment of breast cancer for 90 years until 1981, when Bernhard Fisher proposed his idea, that the combination of adjunct therapy with local surgery may provide a higher survival rate compared to extensive surgical procedures.[42,43]. Cancer removal by surgery, like lobectomy and mastectomy, is still one of the most commonly used practises to remove localised cancer. However, due to advances in this field, surgery is much less invasive. Nowadays, the evolution of cancer treatment took a significant leap forward with the introduction of systemic adjuvant therapies. Among these, radiation and cytostatic drugs played pivotal roles.[44] Only one year after the discovery of X-rays by Roentgen in 1895, ionising radiation was already used to treat cancer. Initially, the limited knowledge of radiation biology, lack of radiation protection and quality control left a lot of patients with severe side effect, but due to advances in the recent decades, external beam radiation and internal treatment is commonly used in cancer therapy.[45] This treatment employs high doses of ionising radiation to target and damage genetic material of cancer cells to interfere with excessive cell division. Combined with other treatment methods like surgery, radiation can be used to shrink the tumour before surgery (neoadjuvant therapy) or after a surgical procedure (adjuvant therapy) to destroy tumour residues.[46] Since high-energy radiation affects both normal and abnormal cell, the goal of radiotherapy is to minimize the damage to surrounding healthy tissues.

Contrary to localized treatments, systemic therapies, including targeted-, immune-, and chemotherapy, are designed to treat cancer cells that may have spread beyond their original site.[47] Systemic therapy drugs are usually administered orally, intravenous or intramuscular, depending on the drugs chemical properties, pharmacokinetics and the desired effect.[45] Conventional chemotherapeutics often aim to disrupt the process of cell division and rely on the ability of normal cells to repair chemotherapy-related damage. Their main drawbacks are limited selectivity, adverse effects, and the development of drug resistance.[5,47] Several metal-based chemotherapeutics are presented and discussed in the next chapter.

1.2.1 Platinum(II) based chemotherapy:

In 1977, American oncologist Lawrence Einhorn reported that, out of 50 patients suffering from advanced testicular cancer, 75% were cured by a three-drug chemotherapy containing cisplatin alone and additional 20% due to a combinational therapy with adjuvant surgery.[48] Just one year later, the small molecule platinum compound cisplatin became the first metalorganic chemotherapeutic that was approved by the food and drug administration (FDA). To this date, the

first-line platinum drugs cisplatin, carboplatin and oxaliplatin (Figure **4**) are still relevant as one of the most applied chemotherapeutics.

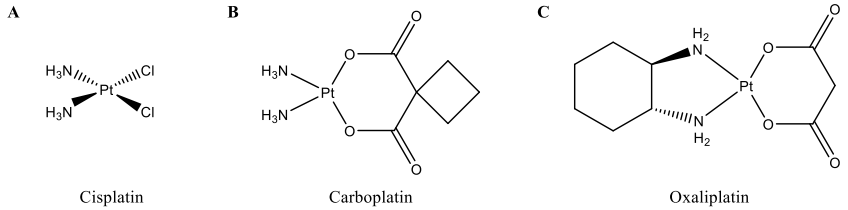

Figure 4: Three major milestones of Pt-based anticancer drugs: A) Cisplatin, B) carboplatin and C) Oxaliplatin

After cisplatin enters the tumour, either by passive diffusion or through the copper transporter CRT1, the complex may be activated by aquation of the chlorido-ligands. The platinum moiety covalently bind to DNA by forming intra- and inter-stranded crosslinks.[49] This is still accepted as the main principle behind the induction of apoptosis. However, other novel mechanisms of action like acidification of the cytoplasm and the disruption of RNA transcription have been uncovered. Compared to the "trailblazer" cisplatin, carboplatin and oxaliplatin exhibit a higher stability due to their bidentate leaving groups, while still maintaining a similar mechanism of action.[50,51]
Platinum-based compounds, including the three commonly used drugs mentioned above, suffer from two major disadvantages: they may induce severe side effects and are susceptible to an acquired drug resistance.[52] These side effects, varying from nausea and vomiting to nephrotoxicity or bone marrow suppression, are attributed to the high toxicity and low specificity of the drug, affecting both malignant and healthy cells.[53] Due to the general structure of cisplatin, the drug offers limited possibilities for modifications regarding tumour specificity, highlighting the importance of finding and developing promising novel, non-platinum based alternatives.[54,55]

1.2.2 Non-platinum based chemotherapeutics:

Over the last decades, pharmaceutical research has worked on exploring alternatives to platinum-based therapeutics. Figure **5** illustrates a comparison between the percentages of scientific papers about Ru-, Au-, Pd-, Ir-, and Rh-based anticancer chemotherapeutics in the PubMed database published in the time period between 2000 to 2021. The data was directly adopted from a review paper by Misso et al.[56] Besides platinum, the platinum-group metal ruthenium has gained the most attention, followed by gold and palladium. Nevertheless, several metallodrugs containing gallium, osmium, iridium, and rhodium have become the subject of intensive investigation and even entered clinical studies.[54,57]

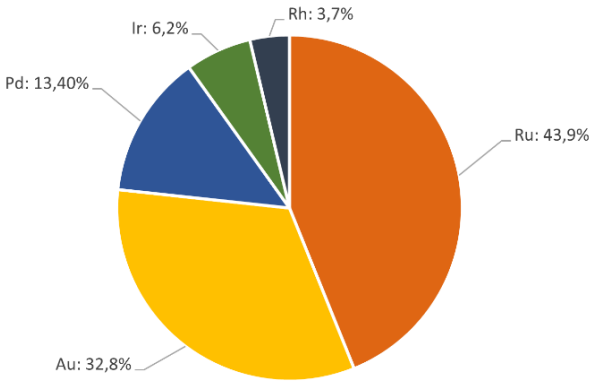

Figure 5: The percentages of papers in the PubMed database about different transition metal complexes and their use as anticancer agents published between 2000 and 2021.

The organometallic compound titanocene dichloride was believed to have a similar mode of action due to the resemblance (Figure **6**, A) with cisplatin, while exhibiting a lower toxicity towards normal cells.[54] Additionally, the compounds higher lipophilicity, attributed to the two cyclopentadienyl (Cp) ligands, may have some significant impact on the pharmacokinetic and pharmacodynamic properties of the drug. In 1993, titanocene dichloride was the first metallocene and non-platinum-based organometallic to enter clinical trials. However, as a result of their low *in vivo* stability solubility, the study was discontinued during phase II since the compound failed to advantages over similar, already established therapies.[54,58]

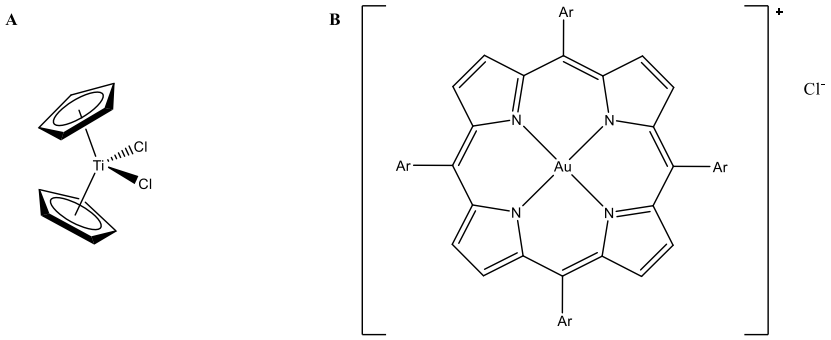

Figure 6: A) Titanocene dichloride and B) the general structure of AuP complexes.

The success of Au^{I}-based therapeutics against rheumatoid arthritis (auranofin/aurothiomalate) set the interest in gold-containing compounds as possible anticancer agents in motion. Gold(I/III) complexes show promising acute toxicity to cells *in vitro*. However low bioavailability, limited stability in acidic milieu and selectivity dampen their clinical application. One way to address these issues involves employing chelating ligands in conjugation with an Au^{III} centre, such as in the case of gold porphyrin (AuP; Figure **6**, B) complexes. They demonstrate favourable chemotherapeutic potential due to remarkable stability under physiological conditions, thereby address one of the major problems of gold-based therapeutics. Their main characteristic ability is

the ability to interact with biomolecules containing a thiol group, allowing the highly selective inhibition of TrxR, a selenoenzyme whose overexpression is associated with aggressive tumour proliferation. Furthermore, other DNA-independent mechanisms, like the increase in intracellular ROS levels and the induction of ER stress have been observed. Still, besides the already established antirheumatic drugs, no novel gold-based chemotherapeutic has yet reached clinical trials for the treatment of cancer.[56,59,60]

In early studies, the "platinoids" rhodium and iridium received less attention considering that they share relatively slow kinetics in terms of ligand exchange, making them much more chemically inert in comparison to similar ruthenium and platinum complexes. Despite that, due to their potent anticancer activity, minimal adverse effects and high water solubility, the interest in these novel drugs persisted and the problem of low bioactivity was approached by the introduction of inherently cytotoxic and substitution-activating ligands.[61,62] Furthermore, researchers have proposed various unique mechanisms that differ from the mode of action of Pt-based chemotherapeutics, making rhodium and iridium-based drugs potential candidates for the treatment of platinum resistant cancer.[63,64]
Besides direct analogues of already established ruthenium complexes and the hydrophobicity-hydrophilicity-balanced Rh^{III}/Ir^{III} half-sandwich compounds, innovative cyclometalated octahedral Ir^{III} complexes which display intrinsic fluorescence gained a lot of attention.[65] These distinctive spectroscopic properties are unique to iridium and enables concurrent bio-imaging applications while still maintaining their mitochondria-targeting properties against cancerous cells.[66]

Ruthenium complexes, as stated previously, are among the most studied alternatives for platinum due to their antineoplastic and antimetastatic properties.[67] Several favourable characteristics of these complexes like enhanced stability and prolonged effectiveness are attributed to their slow dissociation rate *in vivo*. Additionally, the conformational changes caused by ruthenium compounds are usually less pronounced compared to platinum drugs, distorting, and damaging the DNA to a lesser extent and are thereby more reliant on multimodal anticancer mechanisms.[49] NAMI-A (*trans*-imidazoledimethylsulfoxidetetrachloridoruthenate; Figure **7**, C) entered a phase I study in 1999 and is thereby the first ruthenium based therapeutic that entered clinical trials. The major mechanistic difference between most Ru(III) compounds and NAMI-A is, that the latter exhibits a much lower cellular uptake.[68] As a result, NAMI-A shows a remarkable effect on the process of metastasising rather than acting against the primary tumour itself.[69,70] However, due to the emergence of various severe adverse effects, the trial for NAMI-A was terminated.[56]

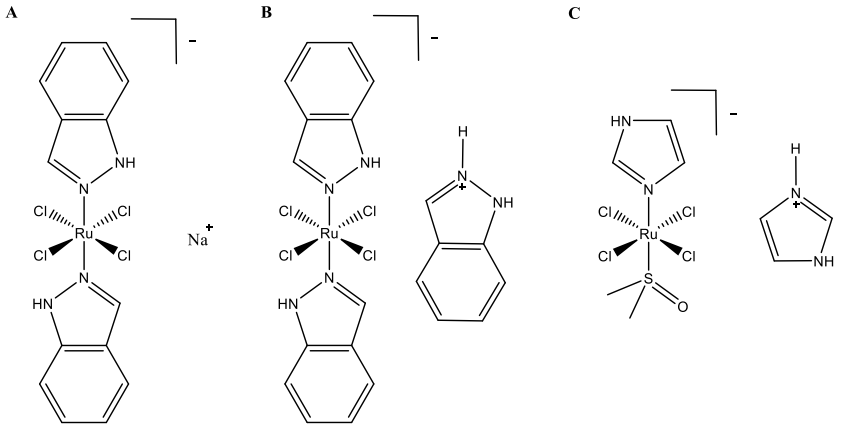

Figure 7: The ruthenium complexes: A) BOLD-100, B) KP1019 and C) NAMI-A

The second ruthenium based anticancer drug to enter clinical trials was KP-1019 (indazolium *trans*-[tetrachloridobis(1H-indazol)ruthenate(III)]; Figure **7**, A), which was developed as a drug against cisplatin-resistant human colon cancer cell lines.[71] It successfully passed phase I without causing any serious side effects. However, due to its poor waster solubility, the focus was redirected to BOLD-100 (sodium *trans*-[tetrachlorobis(1H-indazole)ruthenate(III)]; formerly known as NKP-1339; Figure **7**, B), the more water soluble sodium salt analogue of KP1019.[72,67] According to the Bold Therapeutics Inc. website, accessed in November 2023, BOLD-100 has received Orphan Drug Designations for gastric and pancreatic cancer and is currently in a phase 2 study for advanced colorectal cancer, making it the most clinically advanced ruthenium-based therapeutic currently in development.[73,74] The complex accumulates inside the tumour by binding to several plasma proteins, especially human serum albumin. As a result of the acidic environment inside the tumour, the ruthenium(III) species is activated via reduction to ruthenium(II) and experiences subsequent hydrolysis.[72] Once activated, the drug initiates cell cycle arrest through a multimodal mechanism of action including the induction of endoplasmic reticulum stress by inhibiting the upregulation of the ER chaperone GRP78, as well as the induction of chemically unstable active oxygen species.[75]

1.2.3 Organometallic chemotherapeutics:

The first organometallic drug that was used in experimental chemotherapy was Salvarsan (Arsphenamine), an organoselenium compound, developed by Paul Ehrlich on his pursuit to find the “magic bullet”, a theoretical, highly selective drug that would kill disease-causing agents.[52,76] This marked the beginning of the swift growth in the exploration and creation of antitumor complexes based on metals over the last few decades.

Metal-containing compounds are only classified as “organometallic complexes” if they either contain a metal-carbon σ-bond or a π-bond between the metal center ligand.[52] These substances, including metallocenes, half sandwiched, π-/CO-ligand bonded and carbene derivatives offer

outstanding kinetic stability and biomedical applications.[67] Compared to pure organic chemotherapeutic agents composed of carbon-based structures (e.g. doxorubicin/paclitaxel), organometallic compounds exhibit a far more diverse architecture owning to the high coordination numbers of transition metals. They also demonstrate a strong binding affinity due to the metals intrinsic reactivity in a biological setting and are capable of undergoing a variety of typical chemical transformations due to ligand exchange, which may result in a change of reactivity and novel pharmacological properties depending on their environmental conditions.[77] The bioactivity of an organometallic drug is dependent on the central metal atom, its oxidation state, and the choice of ligands. On account of different ligand exchange kinetics and a wide variety of metal-specific modes of action, it is important to note, that similar metal ions and similar ligands do not directly correlate to similar antitumour activity. Even though titanocene dichloride and cisplatin share a similar structure, titanocene dichloride exhibits distinct modes of action. Furthermore, titanocene dichloride and potential other transition metal drugs may utilise the abnormal high demand of iron, zinc, copper, and calcium, as a selective delivery system into cancer cells as they are involved in many biological processes and are afflicted with active sites of proteins and enzymes.[52,78]

1.2.4. Ruthenium(II) piano stool complexes:

Ruthenium(II) arene complexes are a class of coordination compounds which exhibit a *pseudo*-octahedral geometry resembling a "piano stool". These $[Ru(\eta^6\text{-arene})(X)(Y)(Z)]^{n+}$ complexes possess a metal at the centre, an arene ligand which acts as the seat and either three monodentate, one bidentate and one monodentate or a single tridentate ligand resembling the stools legs.[79] The +2 oxidation state of central atom is stabilised by the *fac*-coordinated arene ring.[80]

Two prominent examples of piano stool complexes are the neutral RAPTA- and the positively charged RAED-class organometallics (Figure **8**). Both incorporate the *p*-cymene to stabilise the Ru(II) ion, a functional ligand and one or two labile chloride ligands which promote the activation of the complex through hydrolysis. RAPTA complexes are distinguished by three monodentate ligands with the labile leaving groups occupying the X and Y position, while the RAED-class contains a bidentate ligand with a single labile ligand. Even though different arene systems have been considered, *p*-cymene has emerged as the dominant choice.[80]

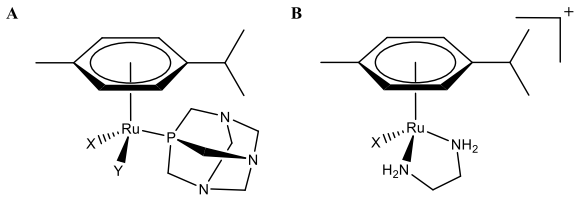

Figure 8: A) RAPTA, developed by Dyson and co-workers; B) RAED, developed by Sadler and co-workers.

Both compound classes share the same activation mechanism through hydrolysis of the Ru-X(/Y) bond under physiological conditions, enabling them to bind to their biological targets. The dissociation of the Ru-X/Y bond can be adjusted based on the selection of ligand Z. Furthermore, neutral Ru(II)-arene complexes (like RAPTA) undergo hydrolysis at a faster rate compared to their cationic counterparts (RAED).[80] The hydrolyzation of RAPTA-C predominantly yields $[Ru(\eta^6\text{-}p\text{-cymene})X(H_2O)(PTA)]^+$. However, aquation of both labile ligands is possible (Figure **9**).[80,81]

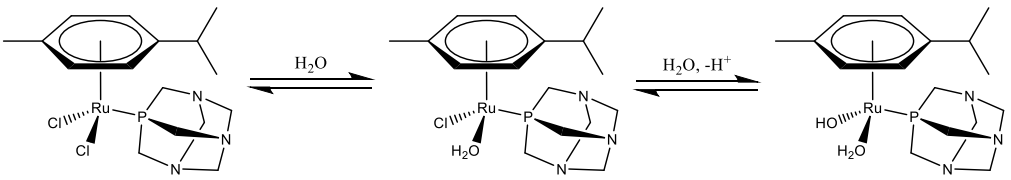

Figure 9: Hydrolysis of RAPTA-C.

Unlike RAPTA-C, which demonstrates metastasis inhibition *in vivo*, RAED-C exhibits significant cytotoxicity and primary tumour activity comparable to cisplatin. The cellular uptake of RAPTA appears to occur through specific interactions with human serum albumin (HSA) and transferrin. Even though a higher lipophilicity increases the cellular uptake, it does not strictly increase the cytotoxicity of the drug. Astarina et al. investigated the influence of different arene rings on the ability of four organometallic RAPTA complexes to inhibit RNA transcription.[82] By increasing the bulkiness of the electron-donating alkyl groups in the arene ring, the reactivity of the compounds towards DNA decreased and reduced the effectiveness in RNA transcription inhibition. This is partly due to the fact that bulkier arene groups induce a higher distortion of the DNA structure, making it easier for the DNA repair machinery to recognise and repair Ru-DNA adducts.[82] The investigation and subsequent comparison of these two organometallic Ru(II)-arene compound classes showcases the versatile characteristics and significant impact of ligand sphere on organometallic compounds, leading to substantial variations in terms of molecular targets and mechanisms of antiproliferative activity.

In 2020, Geisler et al. discovered a novel class of Ru(II) piano stool compounds featuring a unique tridentate *N,O,O*-coordination scaffold while experimenting with various monodentate *N*-donor ligands to increase the stability of KP-2048 (Figure **10**). These tridentate complexes were

synthesised from hydroxy-1,4-naphtoquinone, pyrazole, (cymene)ruthenium dichloride dimer and a vast excess of a base in an one-pot reaction using microwave irradiation.[83]

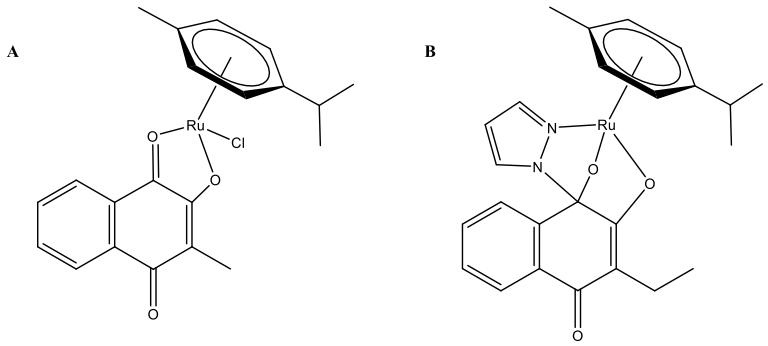

Figure 10: A) KP2048 and B) the novel tridentate ruthenium arene complex(right).

This scaffold includes a hemiaminal bond connecting the C1 carbon of the naphthoquinone and the *N*1 nitrogen of the azole moiety, forming a five-membered ring between the metal centre, the oxygen and the two nitrogens of the 1,2-diazole moiety. The ruthenium(II) metal centre may be exchanged for osmium(II). However, the ruthenium compounds exhibited a marginal increase in their activity compared their osmium analogues.[83] In contrast to their parental compound, these tridentate ligands display increased complex stability in aqueous media besides a remarkable increase of cytotoxicity. This was anticipated since tridentate chelator ligands tend to form more stable complexes than mono- and bidentate ligands in accordance with the "chelate effect".[84] Ligand variation studies were performed for the three different ligands: the positive induction (+I) effect of alkyl chains on the position 3 of the naphthoquinone increased the stability in aqueous media and subsequently the cytotoxicity in a colon (A549) and a lung cancer cell line (SW480). The complex containing an ethyl group showed the highest activity in SW480 lung cancer cell lines with IC_{50} values as low as 57 ± 8 nM.[83] For the "seat ligand", from all tested arene analogues, the *p*-cymene as well as the biphenyl arene yielded the most promising results in colony formation and colorimetric MTT assays. Finally, the formation of the tridentate ligand was only observed with 1,2-diazoles as monodentate ligands.[83,85,86] Accordingly, all complexation experiments conducted in this work were performed with *p*-cymene and 2-hydroxy-3-ethylnaphthalene-1,4-dione.

Due to their rather recent discovery, the complete mechanisms behind their exceptional anticancer activities are still yet not well understood. Neither ROS formation nor plasmid interactions are believed to be responsible for their promising cytotoxicity. Further research on these unusual complexes is necessary to fully uncover the currently enigmatic modes of action.

1.2.5. The important choice of the right ligands:

All things considered, organometallic drugs are of great interest due to the metals distinct features such as redox capability, diverse coordination modes, and reactivity with organic substrates.[78] Nevertheless, despite the promising performance demonstrated by various new organic compounds and transition metal complexes in *in vitro*- and preclinical studies, 90% of all drug candidates entering clinical trials fail, encountering issues like poor aqueous solubility, bioavailability, low efficacy, and severe side effects.[87,88] As briefly addressed in the last two chapters, the right choice of ligands may offer diverse possibilities to address these problems by directly influencing the pharmacological characteristics of a metal complex.[89] Furthermore, the usage of bioactive ligands, which simultaneously impact different targets, may enable multi-target activity to address drug resistance issues.[90] During the hydrolysis process of various metal complexes, one or more ligands might be substituted by water molecules, as seen in Scheme **1**, depicting the hydrolysis process of the tridentate ruthenium(II) complex postulated by Geisler in 2021.[86]

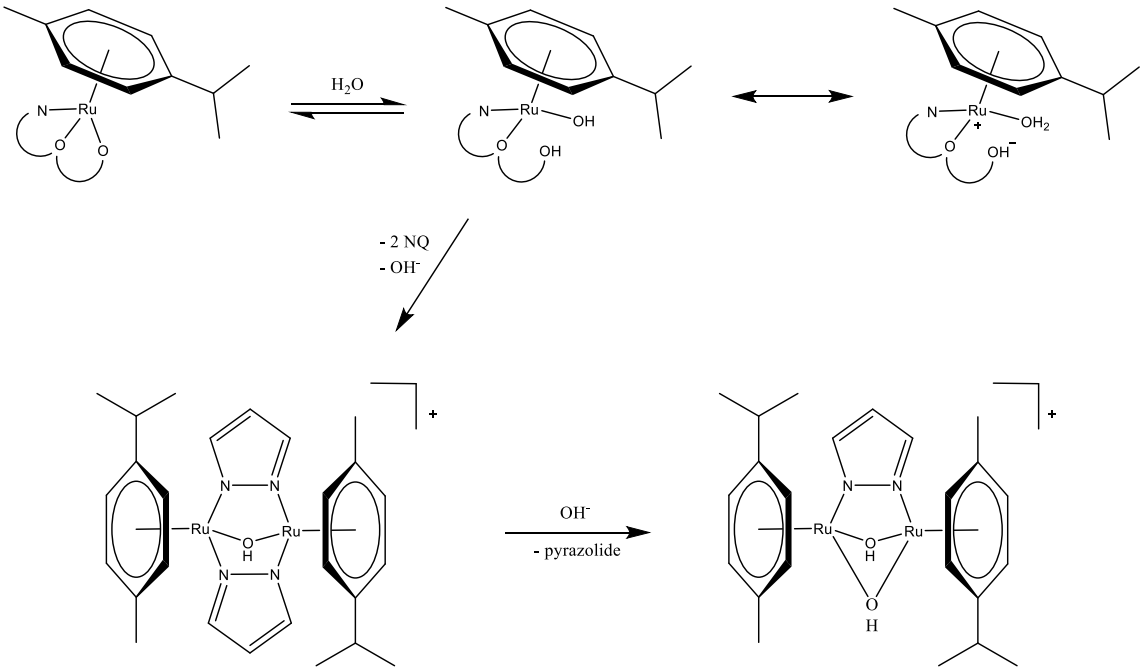

Scheme 1: The postulated hydrolysis mechanism (NQ = Naphthoquinone ligand).

Both ligands are dissociated during the formation of the bis-hydroxido bridged dimer [((*p*-cymene)Ru)$_2$(μ-OH)$_2$(μ-pyrazolate)]$^+$. Once released inside the tumour cells, the unbound ligands can interact with target enzymes and proteins, adding unique modes of action to a drug. In these last two chapters, the bioactivity of the ligands and possible derivatives of the ruthenium compounds are discussed.

1.2.5.1. Naphthoquinone derivatives as bidentate ligands:

Naphthoquinones are a class of organic compounds characterized by a naphthalene ring system connected to a quinone moiety (Figure **11**). They have been the focus of various studies due to their anti-inflammatory, cytotoxic and antiplatelet properties.[91] Fortunately, various derivatives and analogues are commercially available since they are easily synthesised or obtained from natural sources. Several already established organic anticancer drugs contain 1,4-naphthoquinone-like structures (e.g. doxorubicin/daunorubicin), with more naphthoquinone-based organometallics currently under development.[85,92]

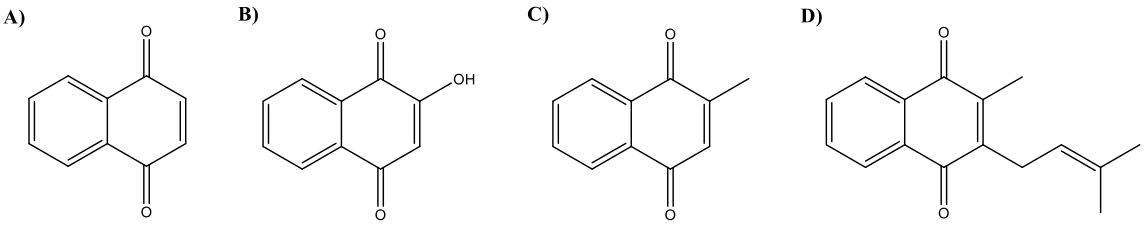

Figure 11: Examples of biologically active secondary metabolites found in plants and fungi.[91] A) 1,4-Naphthoquionen, B) Lawsone, C) Vitamin K_3, D) Lapachole

Naphthoquinones and its derivatives exhibit cytotoxic activities through several different mechanisms like the generation of ROS (reactive oxygen species), induction of apoptosis due to ER stress and the inhibition of topoisomerase I/II.[93] Furthermore, altered expression of the detoxification flavoenzyme NQO1 (NAD(P)H:quinone oxidoreductase 1) has been observed in numerous tumours.[94] Naphthoquinones are believed to inhibit the functions of NQO1 by inducing structural alterations, rendering the enzyme incapable of binding natural substrates.[85] While NQO1 usually demonstrates tumour suppressor properties by modulating the stability of p53, an increased expression of this enzyme may promote enhanced growth in certain cancer cells.[95]

1.2.5.2. Pyrazole and pyrazole derivatives

Pyrazoles, a class of compounds with a five-membered heterocyclic structure, hold significant utility in organic synthesis and stand out as one of the most extensively studied groups within the azole family.[96] Apart from their significance in material and catalytic chemistry, these class of compounds gained a considerable amount of attention in medicinal chemistry owning to their pharmacological profiles.[97] Pyrazole derivatives have demonstrated a wide range of different biological activities like antituberculosis, anticancer, antioxidant, antimicrobial, antiviral and anti-inflammatory.[96,98] Examples of biologically active compounds contain a pyrazole moiety are shown in Figure **12**. Betazole (A) is a histamine H_2 receptor antagonist which is used to stimulate the release of gastric acid in the "Betazole Stimulation Test", a diagnostic procedure for evaluating gastric acid secretion.[99,100] Compound CFI-400936 (B) and SP-600125 (C) are potent tyrosine

threonine kinase inhibitors, a class of enzymes with elevated expression levels in different forms of cancer.[101,102] The nucleoside analogue pyrazofurin (D) exhibits antimicrobial, antiviral and antitumour properties through the inhibition of the natural pyrimidine biosynthesis. Even though the effect of the compound on various types of cancer was demonstrated in rats, pyrazofurin failed to show any tumour regression in any of the 50 patients during the phase I of its clinical trial.[103,104]

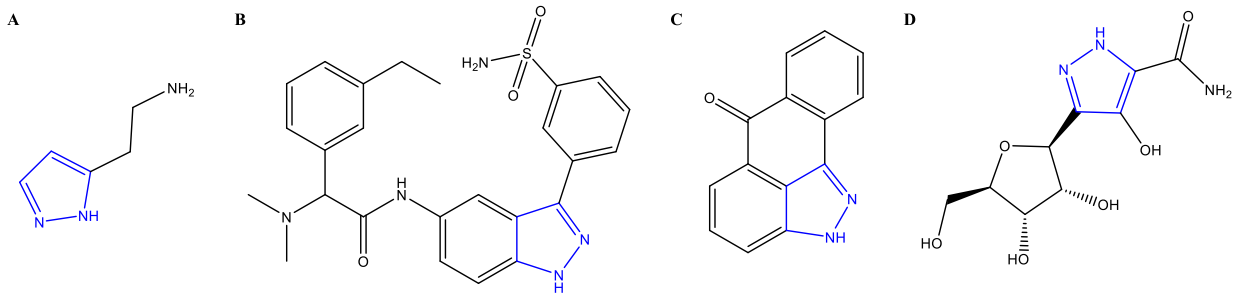

Figure 12: Bioactive compounds containing a pyrazole scaffold.
A) Betazole B) CFI-400936 C) SP-600125 D) Pyrazofurin

The motif that captures significant interest for employing 1*H*-pyrazole as a ligand is the potential Brønsted acidic NH group neighbouring a Schiff-base nitrogen atom. The coordination of pyrazole to a Lewis acidic metal centre increases the acidity of the NH proton, thereby enabling an easier deprotonation.[105] The ensuing pyrazolate anion may then form polynuclear complexes between different metal centres, as depicted earlier in the postulated hydrolysis mechanism in Scheme 1.[97] It is crucial to note that the mandatory requirement for the formation of the tridentate ruthenium(II) complex is the presence of the 1,2-diazole (=N-NH-) scaffold. Therefore, any derivatives featuring substituents on the 1- and 2- positions are deemed unsuitable for this reaction since they would not facilitate the formation of the desired tridentate motif.

Although the compounds outlined in Figure **12** might not be eligible ligands for the tridentate ligand due to steric hinderance or the presence of additional, undesired coordination motifs, understanding the mechanism behind their bioactivity and their behaviour in physiological conditions could proof valuable in the development of novel anticancer agents.

1.2.5.3 The potential of non-cyclic hydrazone ligands

Alternative classes of organic molecules containing the 1,2-diazole motif are non-cyclic hydrazone and *N*-acylhydrazone (NAH, also referred to as hydrazone-hydrazide) derivatives (Figure **13**).[106]

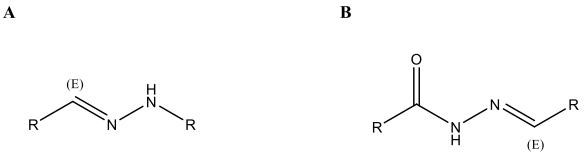

Figure 13: A) The hydrazone and B) N-acylhydrazone motifs.

Hydrazones and NAHs are easily synthesised through a condensation reaction between hydrazide and aldehydes or ketones in protic organic solvents like methanol or ethanol.[107] The conformation of the imide bond (–N=CH–) is relatively constrained and favours the more stable (*E*)-configuration unless the *Z*-diastereoisomer is stabilized through intramolecular interactions.[107–109] However, this means that in theory, a *N*-acylhydrazone can have at least four distinct isomers due to the geometric isomers (*E/Z*) of the C=N double bond and two conformal isomers (*syn/anti*) as a result of the N–N bond.[109] These structural variants may yield pharmacological- and analytical challenge as Polo-Cerón et al. reported that the ^{1}H-NMR spectrum of one of their synthesised NAHs contained multiple duplicated signals due to a mixture of conformers in solution.[110] The four different isomers are shown in Figure **14**.

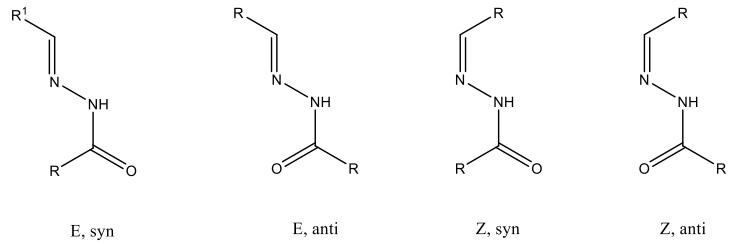

Figure 14:The four isomers and conformers of N-acylhydrazone derivatives.

Nevertheless, this structural motif is still present in the framework of a vast variety of therapeutics for different diseases. One of the most prominent examples of NAH motif containing anticancer drugs is PAC-1 (procaspase-activating compound 1; Figure **15**), a procaspace-3 activating small molecule that selectively induces apoptosis in malignant cells. PAC-1 was discovered by the Hergenrother group during a high-throughput screening in 2006-2008 and completed phase I clinical trials in 2020 for the treatment of advanced malignancies.[107,111–113]

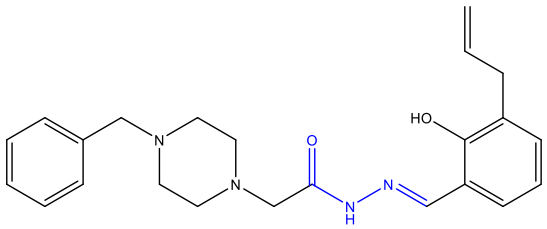

Figure 15: Procaspace-activating compound 1 (CAP-1).

Compared to the hydrazone motif, NAHs feature a more acidic NH proton due to the neighbouring carbonyl group which may facilitate the formation of the tridentate ligand. The simple synthesis and the broad spectrum of biological activities would make these compounds an attractive pharmacophore for future drug design.[109]

2. Results and Discussion

2.1. Aim of this thesis

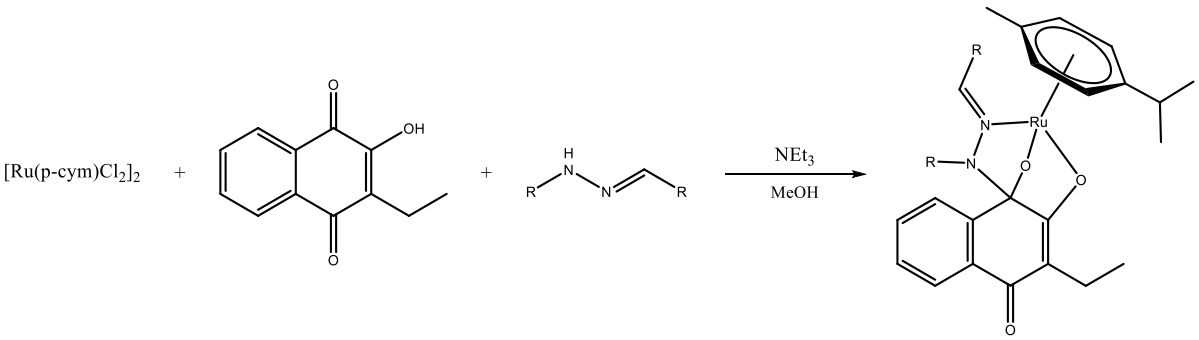

Scheme 2: General reaction scheme for complex synthesis.

The main objective of this thesis was the synthesis and characterization of a range of *N,O,O*-tridentate ruthenium(II) arene complexes with varying *N*-donor moieties. Initially focusing on the influence of different functional groups of substituted pyrazole and indazole derivatives on the complexation behavior of these complexes, non-cyclic hydrazone, and hydrazide ligands should be synthesized and investigated to demonstrating that the 1,2-diazole moiety can be extended beyond the conventional pyrazole ligand for the formation of these novel tridentate complexes. The successful formation of the complexes and their purity should be confirmed through NMR spectroscopy, mass spectrometry and elemental analysis.

2.2. Synthesis of the consistent building blocks

2.2.1. Naphthoquinone and ruthenium dimer synthesis:

First, the dimeric ruthenium(II) arene precursor was synthesized according to literature using ruthenium(III) chloride hydrate and α-terpinene.

For the modified naphthoquinone ligand, a substituent with a positive inductive effect was chosen due to their high stability and cytotoxicity observed in earlier studies.[86] The *O,O*-donor naphthoquinone scaffold acts as a bidentate ligand by forming a five-membered ring after binding to the ruthenium center. The modified naphthoquinone ligand was synthesized by treatment of lawsone with acetaldehyde, L-proline and diethyl 1,4-dihydro-2,6-dimethyl-3,5-pyridinedicarboxylate (Hantzsch ester) and obtained in good yield (83%).

The thereby synthesized 2-hydroxy-3-ethylnaphthalene-1,4-dione (**E2**) and bis[dichloride(η^6-*p*-cymene)ruthenium(II)] (**E1**), in combination with the varying 1,2-diazole ligand, were used as the core structure in all conducted complexation experiments.

2.2.2. Complex syntheses

The first complexation experiments for each ligand were always conducted *via* the synthetic pathway depicted in Scheme **3**. For this procedure, the metal dimer, the naphthoquinone derivative, the respective 1,2-diazole, and an excess of base were stirred in a one-pot reaction under microwave irradiation.

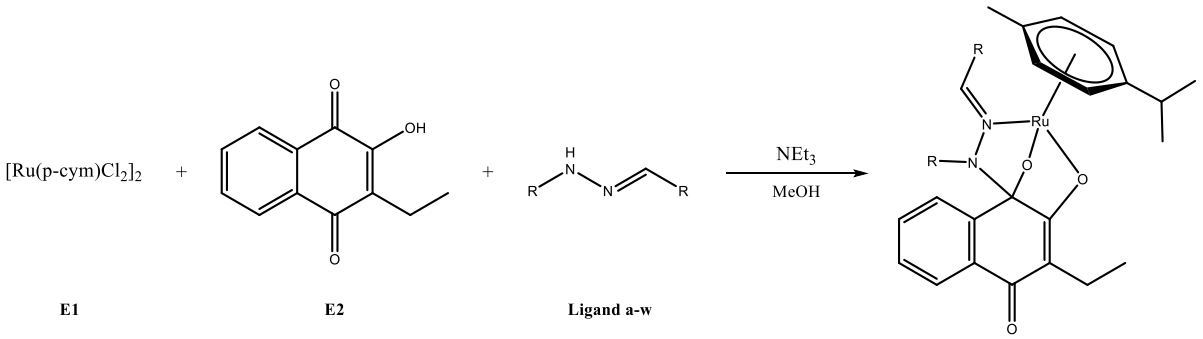

Scheme 3: General complexation reaction.

The prerequisite for the diazole ligand to form the desired triazole structure is the presence of a basic nitrogen neighbouring an acidic *NH*-group. Different scaffolds of 1,2-diazole compounds featuring these characteristics are listed in the following chapters. The formation of the complexes was unambiguously confirmed by the detection of the quaternary carbon C1 around 90–100 ppm in the respective ^{13}C-NMR spectra.[86] Hence, if this peak was observed within the crude ^{13}C-NMR spectrum, a purification of the complex was attempted. Further details on the evaluation of a successful complexation are discussed in the "2.6. Characterization" chapter.

2.3. Variation of the *N*-donor moiety

2.3.1. Complexation of pyrazole derivatives

The first group of molecules, which were tested for their suitability as tridentate ligands, consists of different substituted pyrazole derivatives. For this assessment, three methylated pyrazole ligands (Figure **16**; **a**–**c**) as well as three pyrazole compounds containing distinct electron withdrawing groups (**d**-**f**) were chosen. Compounds **d**–**f** sparked particular interest due to their potential to modify the carbonyl- and halogenide functional groups. All pyrazole derivatives were purchased from common suppliers, as listed under the "3.1.2. Materials" section.

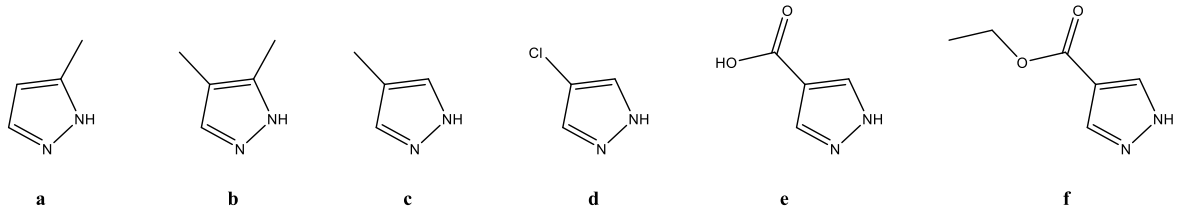

Figure 16: Pyrazole derivatives used for complexation experiments.

Out of the six derivatives displayed in Figure **16**, only the methylated pyrazole derivatives 3-methylpyrazole (**a**), 4-methylpyrazole (**b**), and 3,4-dimethylpyrazole (**c**) lead to a successfully formation of a complex. All three complexes were obtained in good yield (71–82%). Variation of the temperature or the reaction time did not result in a higher conversion rate. The newly formed five-membered ring between the ruthenium metal center, the 1,2-diazole moiety of the ligand as well as coordination to *O*1 and *O*2 to the naphthoquinone ligand, tremendously enhances the stability of the complexes in solution and allows the purification of the complex by standard silica column chromatography with a ternary eluent system. However, due to the acid-susceptibility of the compounds, all column-, as well as thin-layer chromatography experiments had to be performed under basic conditions. Therefore, the acidic silanol groups of the silica gel had to be neutralized with the basic eluent system before loading the crude compound. The purity of the complexes was afterwards confirmed by standard analytical methods. On the contrary, no complexation of the three derivatives featuring an electron withdrawing group (**d**–**f**) could be observed. This may be linked to either the electron withdrawing group reducing the electron density of the heterocycle, thereby preventing the binding of the nitrogen to the metal center or, in case of ligands **e** and **f**, the newly introduced binding sites from the carbonyl group may interfere with the formation of the tridentate motif.

2.3.2. Complexation of indazole derivatives

Following the success of methylated pyrazole ligands, the next step was the introduction of bulkier ligands. The primary target of interest for this scope was the complexation of compound **i** (Figure **17**), a tyrosine kinase inhibitor with diverse pharmacologically significant effects.[102] This molecule may present itself as a promising bioactive ligand for this complex due to the presence of the 1,2-diazole moiety. In order to understand how the different functional groups of this ligand may affect their complexation behaviour, indazole (**g)** and 3-phenyl-1*H*-indazole (**h)** were tested alongside compound **i**. Indazole (**g**) was purchased from Thermo Fischer Scientific, whereas 3-phenyl-1H-indazole (**h**) and 3-iodo-1*H*-indazole, one of the two reagents for the synthesis of compound **i** (Scheme **4**), were synthesized according to literature.[114,115] Before conducting the complexation experiments, the purity of **h** was confirmed by ^{1}H and ^{13}C NMR spectroscopy.

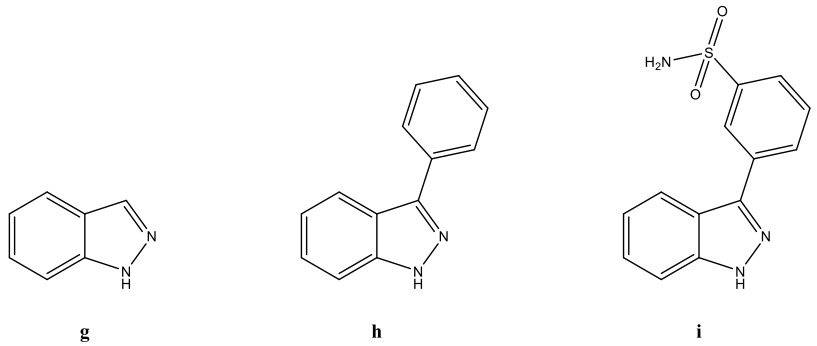

Figure 17: Ligands g) 1H-indazole, h) 3-phenyl-1H-indazole and i) 3-(1H-indazole-3-yl)benzenesulfonamide.

The complexation and subsequent purification of ligand **g** were successful. The complex **IV** was purified by column chromatography. The complexation of **h** led to complex **V** (Figure **18**). However, even after two consecutive purification attempts by column chromatography, the NMR spectra, along with the results of the elemental analysis, still included traces of impurities.

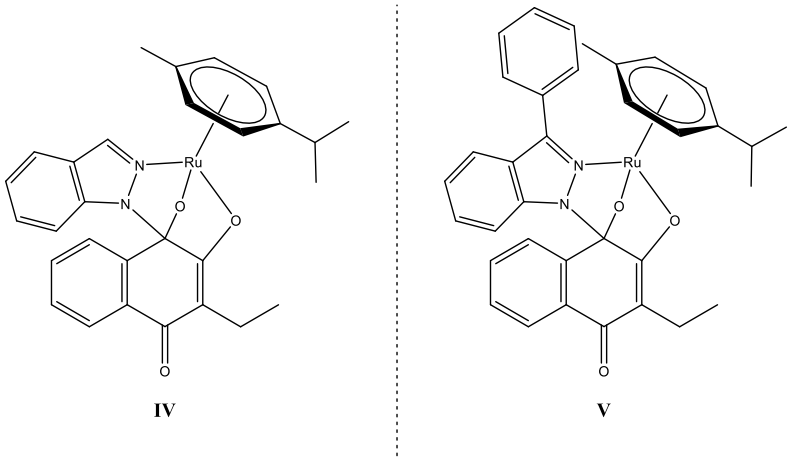

*Figure 18: Only complex **IV** was obtained with satisfying purity.*

The synthesis of compound **i** was attempted *via* a two-step reaction starting with the borylation of 3-bromobenzenesulfonamide, followed by a palladium(0) catalysed Suzuki cross-coupling reaction of the boronate ester and 3-iodo-1H-indazole (Scheme **4**).

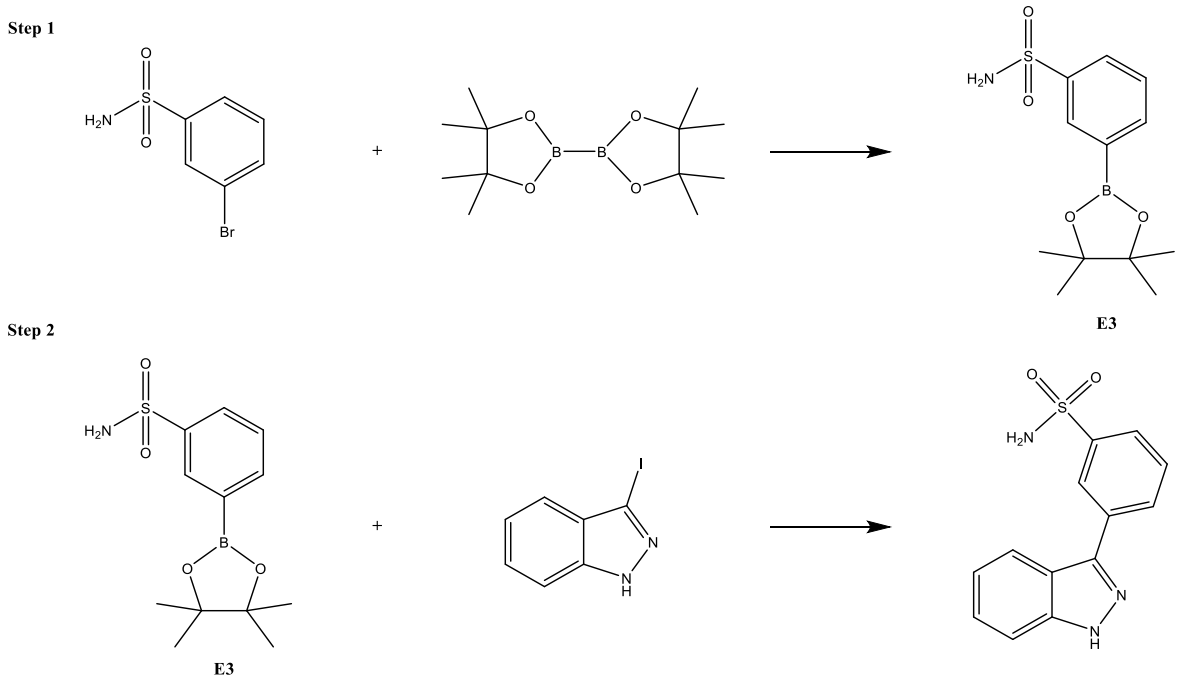

*Scheme 4: Synthesis of compound **i**.*

Unfortunately, both the synthesis and purification of the ligand 3-(1H-indazol-3-yl)benzenesulfonamide failed on three different attempts. Due to the time-consuming nature of synthesizing the starting materials, the research on this ligand was halted. Henceforth, it was not possible to conduct any complexation experiments for this ligand. Despite these challenges, the compound may still be of interest for future studies.

2.3.3. Complexation of triazole, 1,2,3-benzotriazole, 3-methyl-1H-pyrazole-5-one and 2-(methylsulfonamido)thiazole

1,2,4-Triazole (Figure **19**; **j**), 1,2,3-benzotriazole (**k**), and 2-(methylsulfonamido)thiazole (**m**) were the first deviations of the usual 1,2-diazole motif. The compounds **j** and **k** were investigated to assess, whether the introduction of an additional nitrogen atom in the proximity of the hydrazone moiety would interfere with the formation of the tridentate motif. Molecules **j** and **k** were purchased from commercial suppliers while **l** and **m** were synthesized according to literature.[116,117]

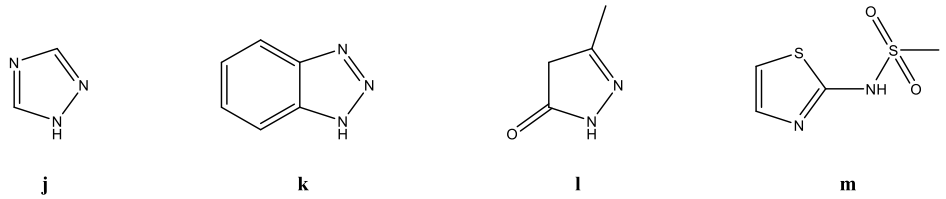

*Figure 19: Ligands **j**–**m**.*

Compound **l** was the first attempt to introduce a carbonyl group into the structure with the intent to increase the acidity of the protonated nitrogen. Additionally, it was anticipated that the methyl group at position 3 would employ a mild electron-inducing effect, thereby increasing the basicity of the nitrogen on position 2. As illustrated in Scheme **5**, 3,5-disubstituted pyrazole was synthesized by Knoevenagel reaction of hydrazine monohydrate and ethyl acetoacetate in good yield (88%). In 2016, Deka et. al. presented an efficient procedure for modification at position 4 of this molecule while remaining the mandatory 1,2-diazole moiety.[118] This procedure may offer a wide variety of substituted five-membered heterocycles as possible ligands with enhanced stability or other beneficial properties.

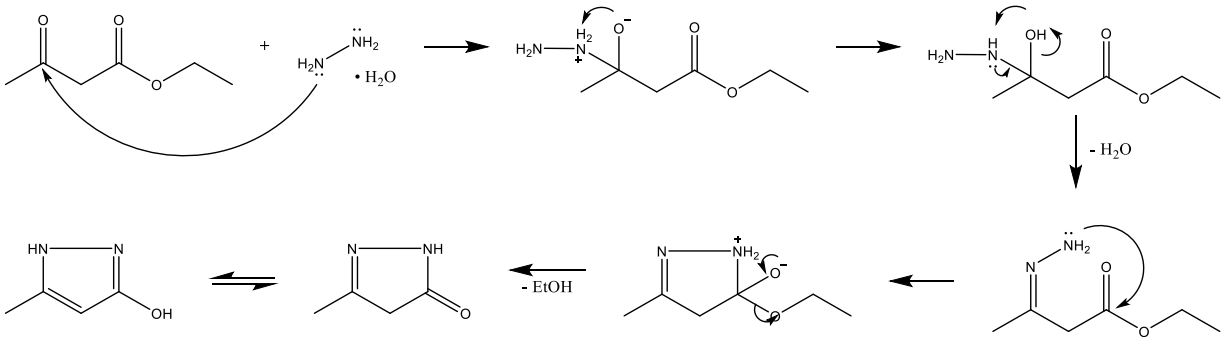

*Scheme 5: The formation of compound **l**.*

Compound **m** was an attempt to replace the novel five-membered ring, which is formed during the reaction between the two ligands and the metal center, with a six membered ring. The compound was synthesized from 2-aminothiazole and mesyl chloride in DCM with an excess of

NEt_3. Previous experiments with 1,3-diazoles were not successful; nevertheless, modifications of this scaffold may offer new possibilities.[83] The idea behind this molecule was, that the nitrogen of the thiazole moiety may coordinates to the ruthenium metal center while the nitrogen of the acidic sulfonamide group would form the hemiaminal bond with the naphthoquinone ligand, as depicted in Figure **20**. However, since there were no indications of complexation observed in the corresponding NMR spectra, the concept of a seemingly less stable six-membered ring was dismissed.

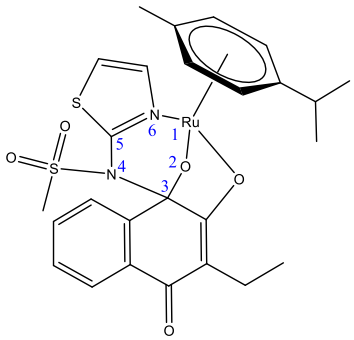

Figure 20: Concept of a complex with a six-membered ring.

In summary, out of the four ligands presented in Figure **19**, only 3-methyl-1H-pyrazole-5-one (**l**) resulted in the formation of the desired motif. The fact that 1,2,4-triazole failed to form a complex led to the hypothesis that the ligand may coordinate with the *N*4 nitrogen to the metal center rather than the *N*2 nitrogen, thereby preventing the formation of the hemiaminal bond due to the absence of the 1,2-diazole moiety.[119] Still, this theory could not be verified, as no NMR spectra or crystal structure of this complex were obtained.

2.3.4. Synthesis and complexation of non-cyclic ligands

After evaluating several cyclic structures, the next motifs of interest involved open-chain hydrazine molecules containing aliphatic or ring systems. Therefore, nine different non-cyclic compounds containing varying substituents were synthesized (Figure **21**). Subsequent complexation should ideally lead to their respective ruthenium(II) complexes.

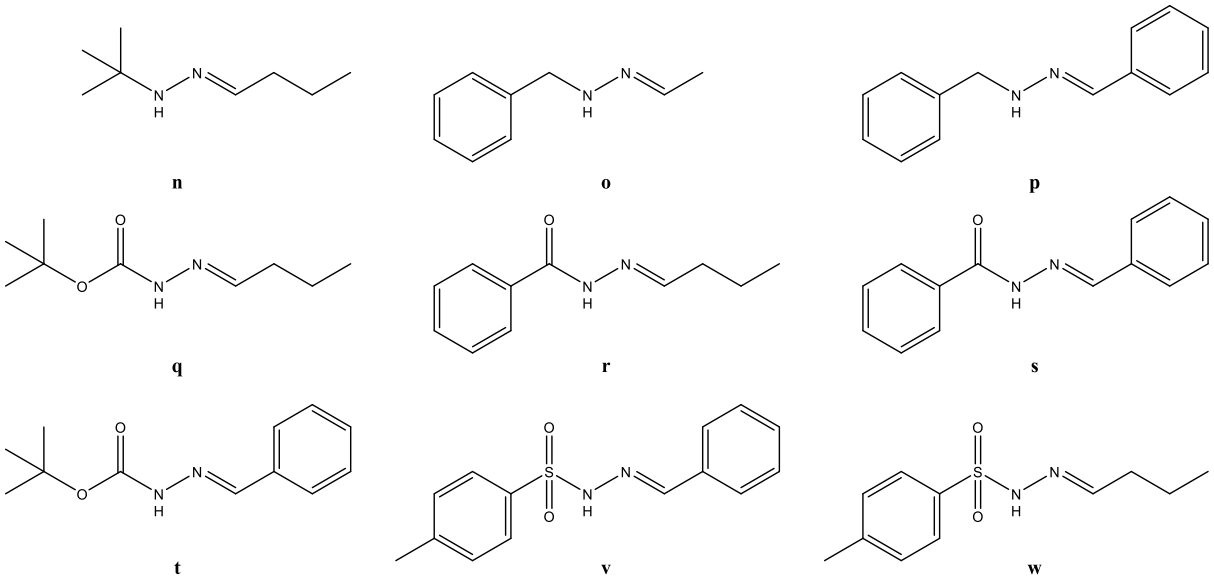

Figure 21: Open-chained 1,2-diazole ligands used for the complexation experiments.

All hydrazine/hydrazide ligands were synthesized according to the general procedure for the hydrazone synthesis and the crude product was purified *via* column chromatography. The general mechanism of formation of the hydrazone/hydrazide ligands is depicted in Scheme **6**. The synthesis of all ligands showed good yield (71–82%). No coherent connection between the length of the ligand and the respective yield was observable. The formation of the ligands was confirmed by mass spectrometry as well as ^{1}H– and ^{13}C–NMR spectroscopy.

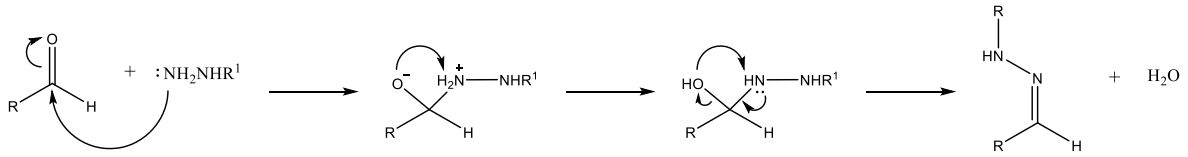

Scheme 6: General mechanism of the hydrazone formation.

The first attempt to use open-chained ligands involved short-chained hydrazine ligands **n** and **o**, intended to structurally mimic the pyrazole moiety, which led to the successful complexation of compounds **a**–**c**. However, the pK_a values and subsequently the reactivity of the nitrogen varies tremendously compared to pyrazole. It was found that the short-chained hydrazone ligands **n** and **o** demonstrated no complexation and this group was therefore discarded. Proceeding with

hydrazine ligands, the introduction of a benzyl group was anticipated to increase the lipophilicity and stability of the complex. Yet, no complexation of these steric demanding hydrazine ligands was observed. Since no hydrazine group formed the desired motif, the next step was to introduce an amide group into the structure to simulate the acidic nature of the pyrazole NH. Hydrazides were promising ligands due to the electron withdrawing group lowering the pKa of the NH moiety. The first tested hydrazide compound was compound **q** which resulted in the first successful complexation with an open-chained ligand of this group. It appears, that the presence of a carbonyl group increases the stability of the tridentate ligand compared to ligands containing a hydrazone structure. Furthermore, comparing the successful complexation of ligands **q** and **r** with the unsuccessful complexation of Ligand **s** and **t** led to the inference that a sterically demanding substituent, originating from the aldehyde group, hinders the formation of the desired tridentate motif. In conclusion, out of all ligands presented in Figure **21**, only Ligand **q** and **r** formed the complexes **VII** and **VIII** (Figure **22**).

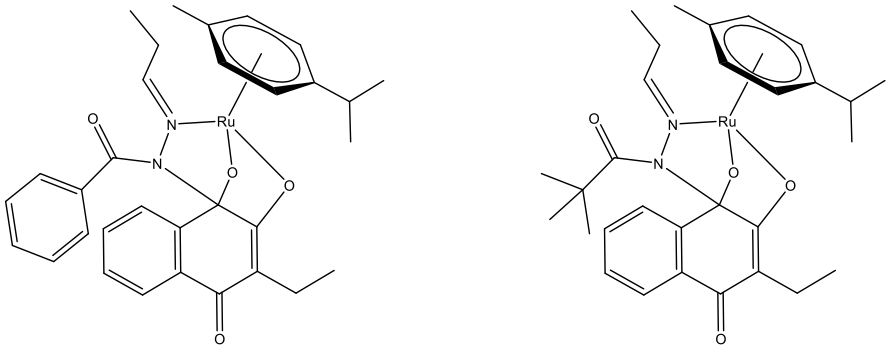

Figure 22: Successful formation of open-chain hydrazide complexes.

Purification of the complexes proved to be challenging due to the complex´s instability compared to the parental compound yielding to decomposition during column chromatography. A common problem that occurred during this purification method was the detachment of the naphthoquinone ligand, even after neutralization of the silica gel, leaving the hydrazone molecule as a bidentate *N,O*-ligand bound to the metal center. Purification *via* column chromatography was attempted with different stationary phases, including silica gel, basic aluminum oxide, neutral aluminum oxide and "deactivated silica gel". The modified silica gel was prepared according to literature by Panne and Fox.[120] However, no improvement in the purification of the complex was observed for any of these column materials. Furthermore, all attempts to purify the complex through precipitation with DCM/*n*-hexane were unsuccessful. The ^{1}H-NMR spectrum of the filtrate showed clear signs of decomposition along with remaining impurities. Furthermore, the use of DCM as a solvent for precipitation or as a component in the mobile phase for column

chromatography resulted in an excess precipitation of a triethylammonium salt. Therefore, the use of DCM was avoided, and all further column purifications were performed with a ternary eluent system (EtOAc/*n*-hexane/NEt_3 or EtOAc/*n*-hexane/NH_4OH).

During the last weeks of practical work, promising yellow solids of the complexes **VII** and **VIII** were isolated while experimenting with different base additions for column chromatography. Single crystals of complex **VII** were obtained from recrystallization with pentane/DCM. Despite the NMR spectra and the mass spectrometry results not being decisive enough, the single crystal X-ray diffraction analysis confirmed the recurring dissociation of the naphthoquinone ligand from the ruthenium metal center. Since the hemiaminal peak was observed in the ^{13}C-NMR spectrum of the crude product, the complex was once again fragmented during the purification process.

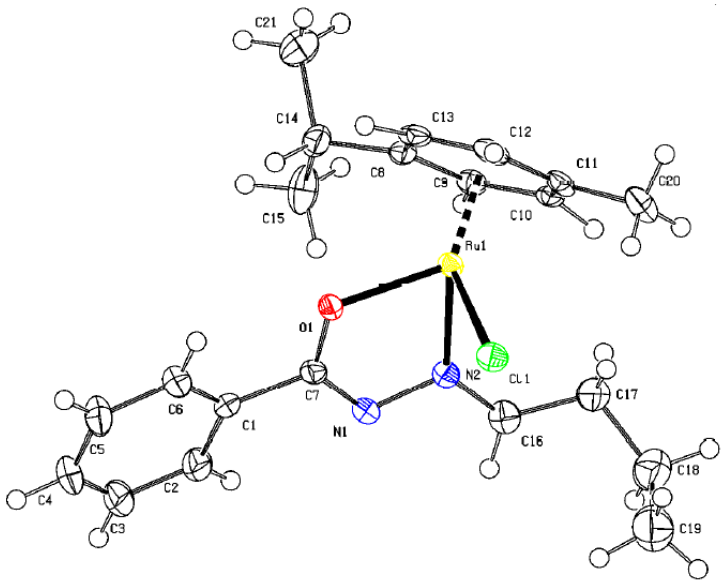

*Figure 23: Molecular structure of the dissociated complex **VIII**.*

2.4. Alternative complexation procedure

The complexation of pyrazole, along with compounds **j**, **q**, **l**, **v**, **s** was additionally conducted through a ligand exchange reaction with the parental naphthoquinone complex featuring a chlorido leaving group (Scheme **7**), similar to the structure of KP2048. The complexation of pyrazole, **q** and **l** were successful. However, this alternative procedure did not result in a higher yield despite requiring a longer reaction time. Nevertheless, both synthetic routes are feasible strategies to obtain these class of complexes.

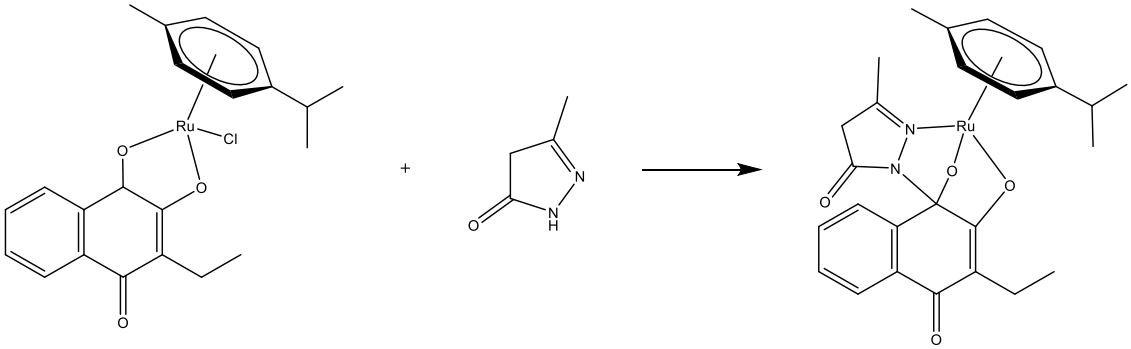

Scheme 7: Complexation of compound l through a ligand exchange reaction.

2.6. Characterization

2.3.1. NMR spectroscopy

NMR spectroscopy studies were carried out on a Bruker Avance III™ HD Ascent 500 Plus spectrometer at 500.10 (^{1}H) and 150.95 (^{13}C) MHz. The solid complexes were dissolved in CD_3OD whereas ligands were measured in DMSO-d_6. The ^{1}H and ^{13}C shifts are referenced in relation to the respective solvent peaks.

2.3.1.1. ^{1}H-NMR spectroscopy of the complexes:

The formation of the desired complex was confirmed by NMR spectroscopy due to the observable changes upon coordination of the ligand scaffolds to the organometallic fragment. Figure **24** depicts the ^{1}H NMR spectrum of complex **II** to illustrate the upfield shift that certain signals experience due to the proton's spatial proximity to the arene ligand.[85]

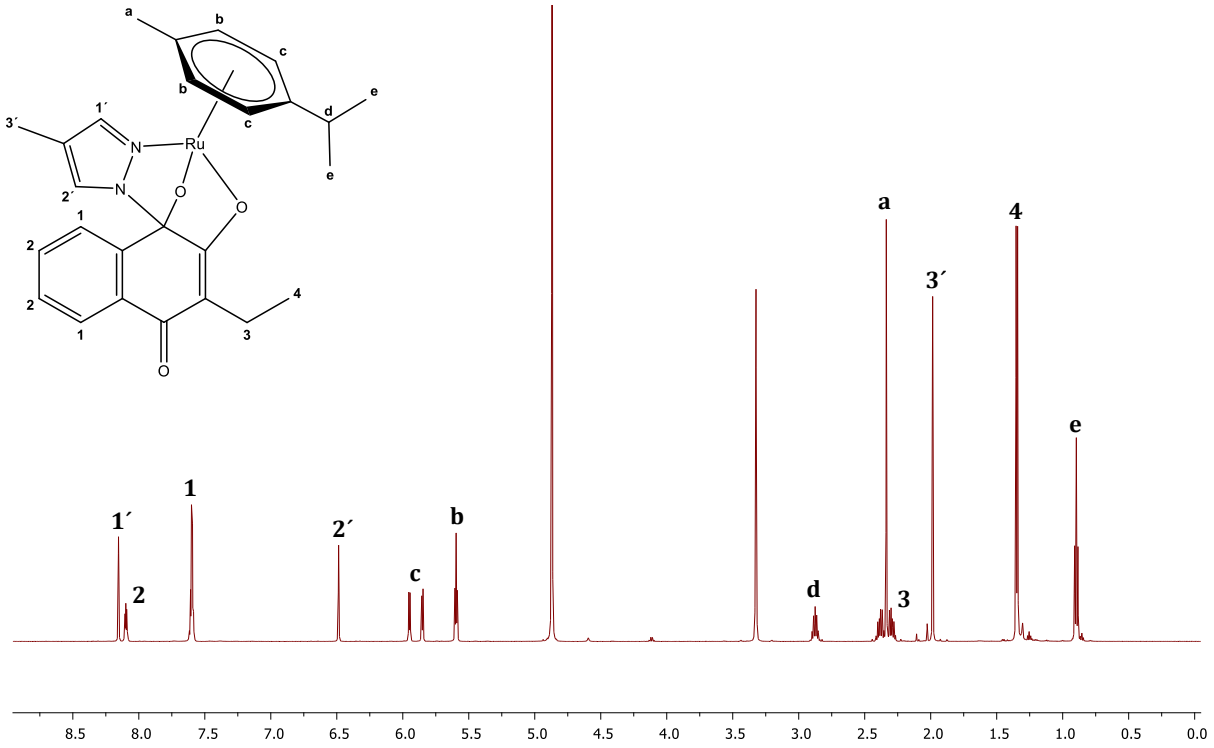

*Figure 24: ^{1}H NMR spectrum of **II** in CD_3OD.*

Of particular interest are the characteristically separated signals of the *p*-cymene between 5.50–6.10 ppm. Literature on bidentate ruthenium(II) arene complexes has reported a split of the aromatic arene proton signals into four doublets due to the restricted rotation of the Ru-cymene bond depending on the size of the coordinated ligands.[121–123] While the majority of the newly synthesized tridentate complexes demonstrated this phenomenon, a few compounds displayed

minor deviations. In the spectra of the complexes **II** and **IV**, only three peaks in this range are visible due to the overlapping of two of the four doublet peaks (Figure **25**; **B** and **C**). The arene protons of compound **II** (**B**) exhibit a seemingly triplet signal with a twofold intensity, whereas complex **IV** (**C**) shows a single doublet. To confirm that these interfering signals are two separate peaks, the spectra may be recorded with different solvents, preferably by exchanging the protic solvent with an aprotic one or *vice versa*.

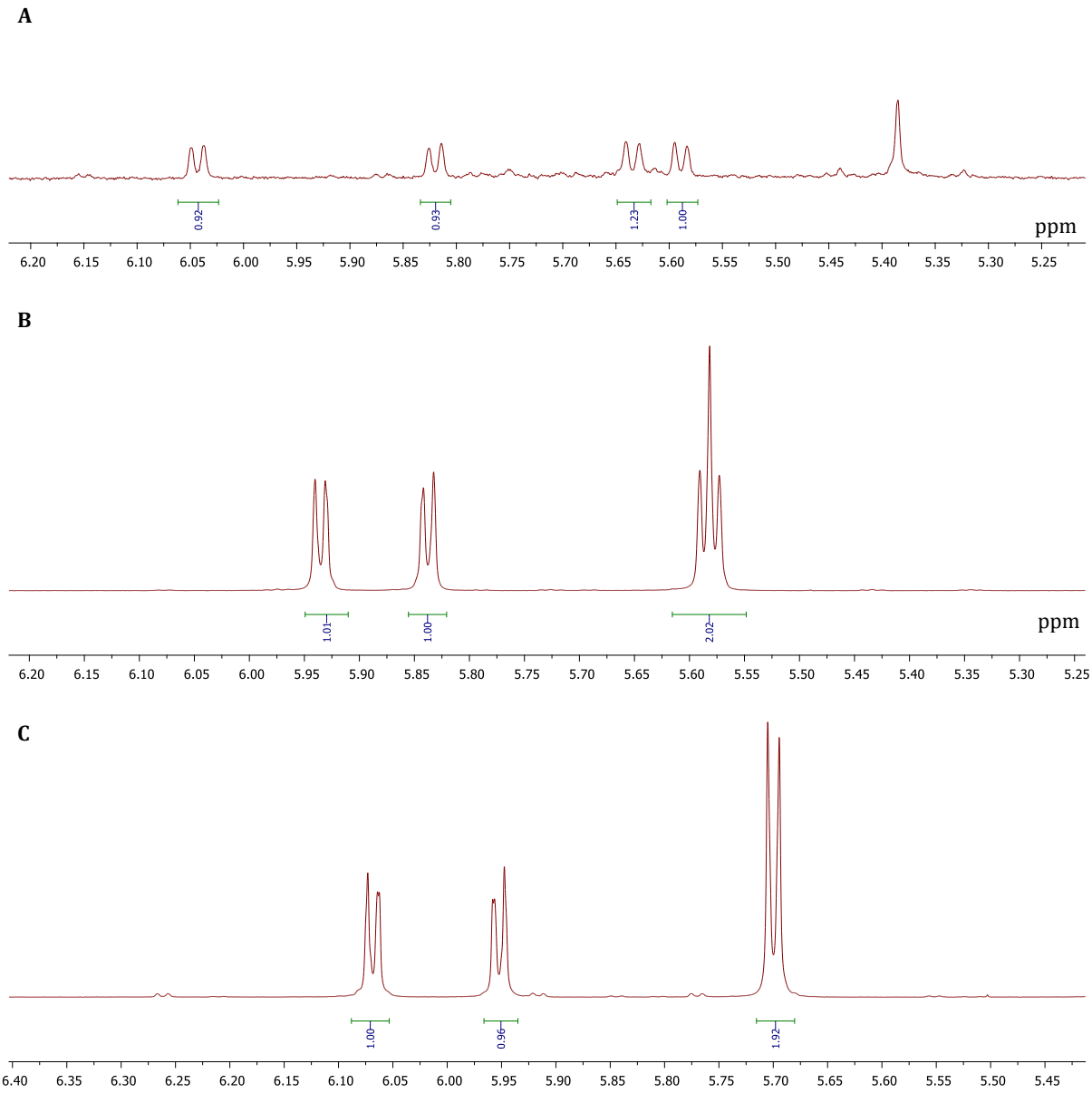

*Figure 25:[1]H NMR spectra in the range between 5.50-6.10 ppm of complexes A) **VI**, B) **II** and C) **IV***

Another noteworthy observation in the [1]H-NMR spectra of the complexes **I** and **III** is the presence of second set of peaks between 5.50–6.10 ppm, as seen in Figure **26**. These additional, shifted signals exhibit a decreased intensity compared to the primary set. This was only observable for the four arene protons as no other peak in the spectra displayed this behavior.

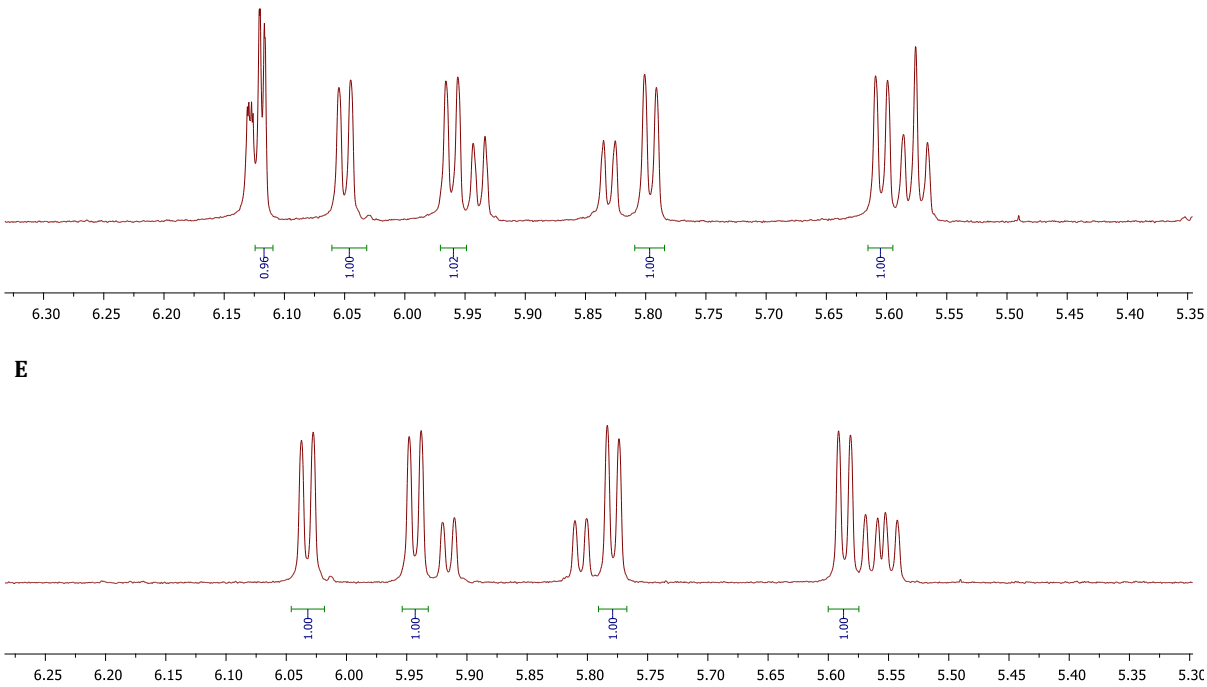

*Figure 26: ^{1}H NMR spectra in the range between 5.50-6.10 ppm of complexes D) **I** and E) **III**.*

Previous studies on ruthenium piano stool complexes containing bidentate, non-cyclic ligands linked this occurrence to diastereoisomers within the structure of the complexes.[124] In 2022, Martínez-Estévez and García-Fontán identified a second set of signals in the spectra of two complexes, attributing them to *E/Z* isomers of an iminic bond in the thiosemicarbazone bidentate ligand.[125] However, as the cyclic 3-methylpyrazole and 3,4-dimethylpyrazole are constrained in the *Z* configuration, the formation of the *E* isomer is not possible. The same restriction seems to apply to the open-chained ligands **q** and **r**, where the imine group, which would exhibit *E*/*Z* isomers in their unbound form, is presumably incapable of isomerization due to steric hindrance from the arene group.

A conceivable explanation for this observation would be the partial hydrolysis of one or more unidentified bonds from the dissolved complex due to the presence of water in the NMR sample. Alternatively, the resonance structure of pyrazole derivates may allow the diazole ligand to either bind through the N1 or N2 to the ruthenium center. Symmetric pyrazole ligands, such as pyrazole or 4-methylpyrazole, only exhibit one binding pattern due to their resonance structure. In contrast, asymmetrical substituted pyrazole derivates like 3-methylpyrazole and 3,4-dimethylpyrazole feature two binding sites, resulting in readily distinguishable regioisomers with distinct sets of NMR signals (Figure **27**). This theory would furthermore infer that the electron withdrawing effect stemming from the carbonyl group in compound **l** and the open-chained hydrazide ligands **q** and **r** would prevent the binding of the N2 atom to the ruthenium center as no second set of signals for the complexes **VI-VIII** was observed.

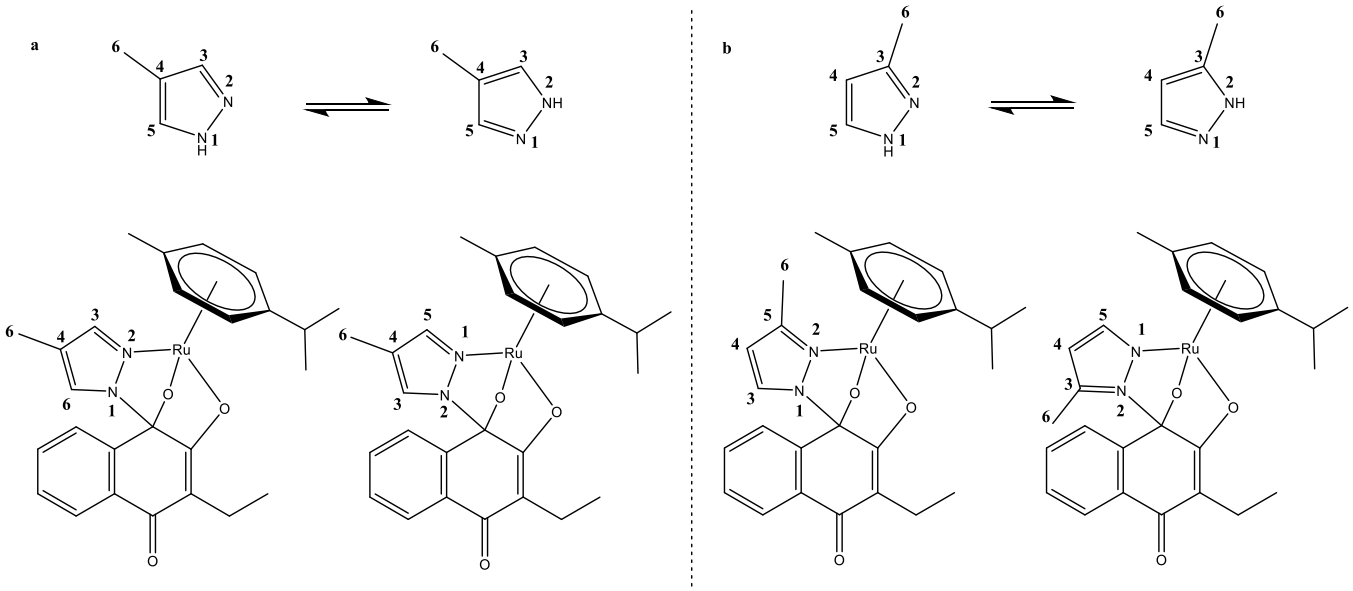

Figure 27: Different binding motifs of a) 4-methylpyrazole b) 3-methylpyrazole.

Nevertheless, this hypothesis remains speculative. Stability tests, NMR spectra at different temperatures or crystal structures of the complexes **I** and **II** are necessary to make further statements about this topic. However, these tests were not included in the scope of this work.

2.3.1.2. ^{13}C-NMR spectroscopy

As briefly mentioned, the ^{13}C-NMR spectra of the complexes are another vital tool to verify the successful formation of the desired complexes. Alongside the strong upfield shift of the coordinated diazole and the *p*–cymene signals, the low intensity peak originating from the quaternary carbon **1** around 90-100 ppm was used as a reference point for the hemiaminal bond formation between the naphthoquinone- and the 1,2-diazole moiety (Figure **28**). Furthermore, just as observed within the ^{1}H-NMR spectra, the arene signals are split into separate peaks due to the locked symmetry in the complex.[125]

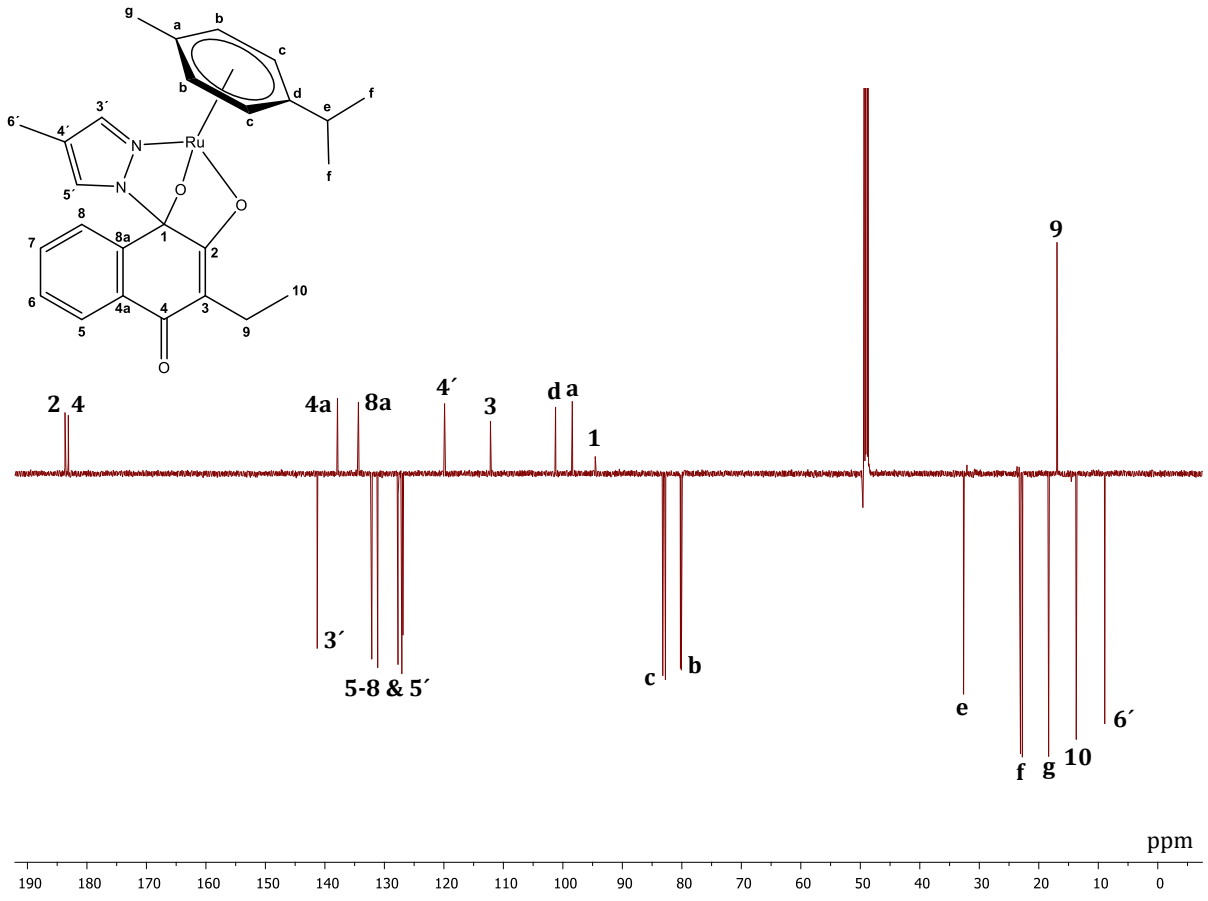

*Figure 28: ^{13}C-NMR spectrum of complex **II** in CD_3OD.*

3. Experimental Part

3.1. Equipment and Materials

3.1.1. Equipment

Microwave	Biotage® Initiator+
NMR spectrometer	600.25 MHz (AV III 600 Bruker BioSpin) 500.32 MHz (AV NEO 500)
Mass spectrometer	amazon speed EDT – mass accuracy routinely < ±2 Da
Elemental analysis:	Microanalytical Laboratory of the University of Vienna, PerkinElmer 2400 Series II CHNS/O Elemental Analyzer for CHNO analyses.

3.1.2. Materials

Solvents, drying agents, and adsorbents were purchased from commercial suppliers and used without further purification unless otherwise noted.

A list of chemicals used and their respective suppliers: 2-hydroxy-1,4-naphthochinon (Acros Organics), p-toluenesulfonhydrazide (Acros Organics), α-terpinene (Alfa Aesar), 4-chloro-1H-pyrazole (AmBeed), 3-methylpyrazole (AmBeed), 3,4-dimethyl-1H-pyrazole (AmBeed), ruthenium(III) chloride hydrate (Johnson Matthey), 2- aminothiazole (Sigma Aldrich), acetaldehyde (Sigma Aldrich), benzhydrazide (Sigma Aldrich), benzylhydrazine dihydrochloride (Sigma Aldrich), L-proline (Merck), 3-bromobenzenesulfonamide (TCI), ethyl acetoacetate (TCI), ethyl 4-pyrazolcarboxylate (TCI), butyraldehyde (TCI), *tert*-butylcarbazate (TCI), bis(pinacolato)diborane (TCI), indazole (Thermo Fischer Scientific), triethylamine (Thermo Fischer Scientific).

3.2. Ligand Synthesis

3.2.1. 2-Hydroxy-3-ethylnaphthalene-1,4-dione (**E2**):

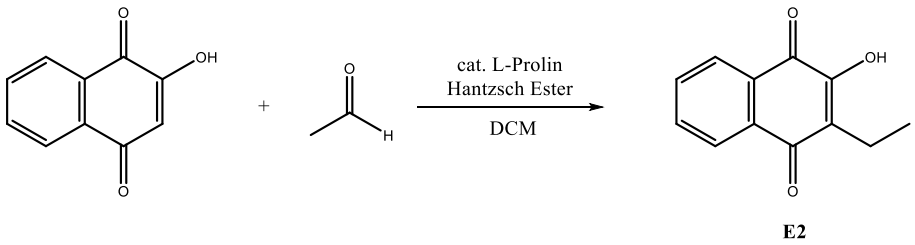

Figure 29: Synthesis of 2-Hydroxy-3-ethylnaphtalene-1,4-dione.

Lawsone (1.01 g, 5.90 mmol, 1.00 eq.), acetaldehyde (645 µL, 11.5 mmol, 1.95 eq.) and Hantzsch ester (1.50 g, 5.92 mmol, 1.00 eq.) were dissolved in 20 mL DCM and stirred at room temperature for five minutes. L-Proline (133 mg, 1.15 mmol, 0.20 eq.) was added and the reaction mixture was stirred under microwave irradiation at 85°C for 25 minutes. The reaction mixture was washed with 10% HCl and brine. The organic layer was dried over anhydrous sodium sulfate and the solvent was removed under reduced pressure. The resulting red viscous oil was purified by column chromatography (silica, gradient 60–80% ethyl acetate in n-hexane) and the product was dried in *vacuo*. The naphthoquinone derivate **E2** was obtained as a yellow solid in good yield (990 mg, 4.90 mmol, 83%).

^{1}H-NMR (500 MHz, $CDCl_3$): δ 8.12 (dd, J = 7.6, 0.8 Hz, 1H, CH: arom.), 8.08 (dd, J = 7.6, 0.8 Hz, 1H, CH: arom.), 7.75 (ddd, J = 7.6, 7.5, 1.3 Hz, 1H, CH: arom.), 7.68 (ddd, J = 7.6, 7.5, 1.3 Hz, 1H, CH: arom.), 7.29 (s, 1H, OH), 2.63 (q, J = 7.6 Hz, 2H, CH_2), 1.15 (t, J = 7.5 Hz, 3H, CH_3) ppm.

3.2.2. Bis[dichlorido(*η6-p*-cymene)ruthenium(II)] (**E1**):

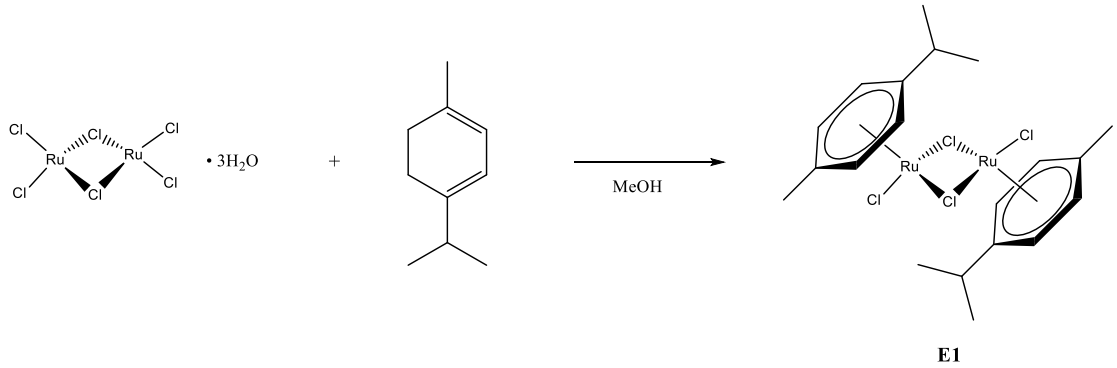

Figure 30: Synthesis of the ruthenium dimer Bis[dichlorido(η6-p-cymene)ruthenium(II)].

$RuCl_3$ •$3H_2O$ (1.00g, 3.83 mmol, 1.00 eq.) was dissolved in 20 mL Methanol and α-terpinene (3.10 ml, 19.1 mmol, 5.00 eq.) was added. The reaction mixture was stirred under microwave irradiation for 30 seconds at 140 °C. The content of the microwave vial was transferred into a 100 mL round bottom flask, which was then filled with DCM and stored in the freezer overnight to complete precipitation. The dark red precipitate was washed with DEE (3 × 10ml) and dried under vacuum (1.77g, 2.89 mmol, 75%).

^{1}H-NMR (500 MHz, MeOD): δ 5.86 (d, J = 6.0 Hz, 4H, CH: arom.), 5.64 (d, J = 5.9 Hz, 4H, CH: arom.), 2.76 (hept., J = 6.9 Hz, 2H, CH), 2.18 (s, 6H, CH_3), 1.29 (d, J = 7.0 Hz, 12H, CH_3) ppm.

3.3. General ligand synthesis procedure

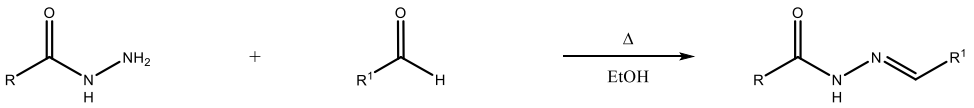

Figure 31: Ligand synthesis: general procedure.

The hydrazide derivative (1.00 eq.) and the respective aldehyde (1.00 eq.) were dissolved in 15–30 mL ethanol and stirred under reflux for 19–25 h. After cooling to room temperature, the solvent was removed under reduced pressure and the pure hydrazone product was obtained through purification by column chromatography.

3.3.1. tert-Butyl 2-butylidenehydrazinecarboxylate (**q**):

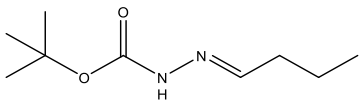

*Figure 32: Ligand **q**.*

Following the general procedure, *tert*-butyl carbazate (150 mg, 1.10 mmol, 1.00 eq.) and butyraldehyde (99.4 µl, 1.10 mmol, 1.00 eq.) were dissolved in 15 mL ethanol and stirred at 90 °C for 20 h. The solvent was removed under reduced pressure and the solid was purified by column chromatography (silica, gradient 10–30% EtOAc in *n*-hexane + 5% NEt_3) to yield ligand **q** as a colourless solid (160 mg, 0.86 mmol, 78%).

^{1}H-NMR (500 MHz, $CDCl_3$): δ 7.21 (t, J = 5.7 Hz, 1H, N=CH), 2.19 (q, J = 7.5 Hz, 2H, CH_2), 1.50 (h, J = 7.5 Hz, 2H, CH_2), 1.47 (s, 9H, CH_3). 0.93 (t, J = 7.4 Hz, 3H, CH_3) ppm.

MS (ESI): calculated for $C_9H_{18}N_2O_2$ $[M + Na]^+$: 209.13; found: 209.13

3.3.2. N´-butylidenebenzohydrazide (**r**):

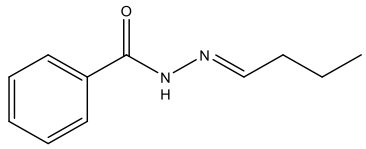

*Figure 33: Ligand **r**.*

Following the general procedure, benzhydrazide (121 mg, 0.89 mmol, 1.00 eq.) and butyraldehyde (79.5 µL, 0.88 mmol, 1.00 eq.) were dissolved in 15 mL ethanol and stirred at 90 °C for 24 h. The solvent was removed under reduced pressure and the solid was purified by column chromatography (silica, 95% EtOAc + 5% NEt_3) to yield ligand **r** as a colourless solid (134 mg, 0.71 mmol, 79%).

TLC (87.5:7.5:5 EtOAc:*n*-hexane:NEt_3) R_f = 0.81 (UV)

^{1}H-NMR (500 MHz, DMSO): δ 11.42 (s, 1H, NH), 7.84 (d, J = 7.4 Hz, 2H, CH: arom.), 7.73 (dd, J = 5.5, 5.5 Hz, 1H, CH: arom.), 7.56 (dd, J = 7.4, 7.4 Hz, 1H, N=CH), 7.49 (dd, J = 7.5, 7.5 Hz, 2H, CH: arom.), 2.24 (q, J = 7.4 Hz, 2H, CH_2), 1.52 (h, J = 7.4 Hz, 2H, CH_2), 0.93 (t, J = 7.4 Hz, 3H, CH_3) ppm.

MS (ESI): Calculated for $C_{11}H_{14}N_2O$ $[M+nH]^+$: 191.12, found:191.11

3.3.3. Benzaldehyde benzoylhydrazone (**s**):

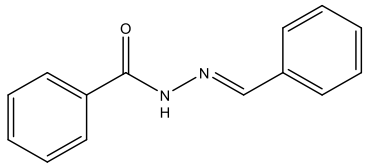

*Figure 34: Ligand **s**.*

Following the general procedure, benzhydrazide (102 mg, 0.75 mmol, 1.00 eq.) and benzaldehyde (75 µL, 0.74 mmol, 0.99 eq.) were dissolved in 15 mL ethanol and stirred at 90 °C for 21 h. The solvent was removed under reduced pressure and the solid was purified by column chromatography (silica, gradient 40–60% EtOAc in *n*-hexane) to yield ligand **s** as a colourless solid (119 mg, 0.53 mmol, 71%).

^{1}H-NMR (500 MHz, DMSO): δ 11.86 (s, 1H, NH), 8.46 (s, 1H, N=CH), 7.91 (d, J = 7.4 Hz, 2H, CH: arom.), 7.73 (d, J = 6.7 Hz, 2H, CH: arom.), 7.59 (dd, J = 7.5, 7.5 Hz, 2H, CH: arom.), 7.49–7.41 (m, 3H, CH: arom.) ppm.

MS (ESI): Calculated for $C_{14}H_{12}N_2O$ $[M+nH]^+$: 225.10, found: 225.10

3.3.4. tert-Butyl 3-benzylidenecarbazate (**t**):

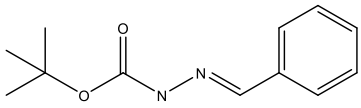

*Figure 35: Ligand **t**.*

Following the general procedure, *tert*-butyl carbazate (150 mg, 1.10 mmol, 1.00 eq.) and benzaldehyde (112 µL, 1.10 mmol, 1.00 eq.) were dissolved in 15 mL ethanol and stirred at 90 °C for 20 h. The solvent was removed under reduced pressure and the solid was purified by column chromatography (silica, gradient 30–40% EtOAc in *n*-hexane) to yield ligand **t** as a colourless solid (198 mg, 0.90 mmol, 82%).

^{1}H-NMR (500 MHz, DMSO): δ 10.91 (s, 1H, NH), 7.99 (s, 1H, N=CH), 7.58 (d, J = 6.82 Hz, 2H, CH: arom.), 7.47 – 7.30 (m, 3H, CH: arom.), 1.46 (s, 9H, CH_3) ppm.

MS (ESI): Calculated for $C_{12}H_{16}N_2O_2$ $[M - H]^-$: 218.11; found: 218.95

3.3.5. N´-benzylidene-4-methylbenzenesulfonohydazide (**v**):

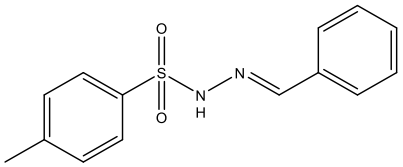

*Figure 36: Ligand **v**.*

Following the general procedure, *p*-toluenesulfonyl hydrazide (122 mg, 0.66 mmol, 1.00 eq.) and benzaldehyde (68.4 µL, 0.66 mmol, 1.00 eq.) were dissolved in 15 mL ethanol and stirred at r.t. for 20 h. The solvent was removed under reduced pressure and the solid was purified by column chromatography (silica, gradient 40–60% EtOAc in *n*-hexane) to yield ligand **v** as a colourless solid (139 mg, 0.51 mmol, 77%).

^{1}H-NMR (500 MHz, DMSO): δ 11.37 (s, 1H, NH), 7.89 (s, 1H, N=CH), 7.76 (d, J = 7.4 Hz, 2H, CH: arom.), 7.55 (dd, J = 7.4, 7.4 Hz, 2H, CH: arom.), 7.43 – 7.37 (m, 5H, overlapping CH: arom. peaks), 2.36 (s, 3H, CH_3) ppm.

MS (ESI): Calculated for $C_{14}H_{14}N_2O_2S$ $[M+nH]^+$: 275.08, found: 275.08

3.3.6. N´-butylidene-4-methylbenzenesulfonhydrazide (**w**):

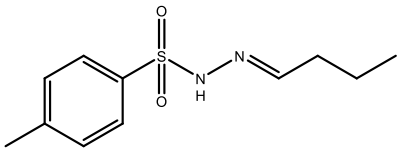

*Figure 37: Ligand **w**.*

Following the general procedure, *p*-toluenesulfonyl hydrazide (121 mg, 0.66 mmol, 1.00 eq.) and butyraldehyde (58.1 µL, 0.64 mmol, 0.97 eq.) were dissolved in 15 mL ethanol and stirred at r.t. for 23 h. The solvent was removed under reduced pressure and the viscous oil was purified by column chromatography (silica, gradient 40–60% EtOAc in *n*-hexane + 5% NEt_3) to yield ligand **w** as a colourless solid (82 mg, 0.34 mmol, 53%).

^{1}H-NMR (500 MHz, DMSO): δ 11.37 (s, 1H, NH), 7.72 (d, J = 7.4 HZ, 2H, CH: arom.), 7.45 (d, J = 7.4 Hz, 2H, CH: arom.), 7.32 (dd, J = 7.4, 7.4 Hz, 1H, N=CH), 2.32 (s, 3H, CH_3), 2.20 (q, J = 7.4 Hz, 2H, CH_2), 1.52 (h, J = 7.5 Hz, 2H, CH_2), 0.93 (t, J = 7.4 Hz, 3H, CH_3) ppm.

MS (ESI): Calculated for $C_{11}H_{16}N_2O_2S$ $[M+nH]^+$: 241.10, found: 241.10

3.3.7. 3-Methyl-1H-pyrazol-5-one (**l**):

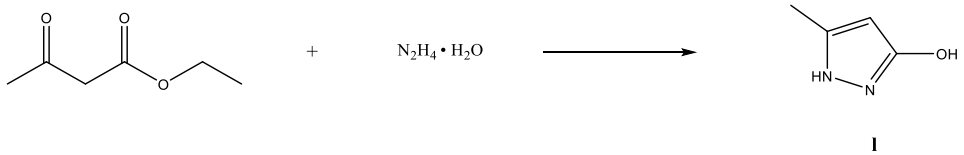

l

*Figure 38: Synthesis of Ligand **l**.*

The flask was charged with ethyl acetoacetate (380 µL, 3.00 mmol, 1.00 eq.) in 10 mL ethanol and hydrazine monohydrate (146 µL, 3.00 mmol, 1.00 eq.) was added dropwise. The reaction mixture was heated under reflux for 20 hours. While cooling to room temperature, the desired compound started to precipitate as a colourless solid. The crude product was filtrated and purified by column chromatography (silica, gradient 60-70% ethyl acetate in *n*-hexane) to yield ligand **l** as a pale-yellow solid (259.3 mg, 2.72 mmol, 88% yield).

^{1}H-NMR (500 MHz, DMSO): δ 11.56 (s, 1H, NH), 9.31 (s, 1H, OH), 5.20 (s, 1H, CH), 2.07 (s, 3H, CH_3) ppm.

MS (ESI): Calculated for $C_4H_6N_2O$ $[M + H]^+$: 99.06, found: 99.05

3.3.8. N´-(thiazol-2-yl)methanesulfonamide (**m**):

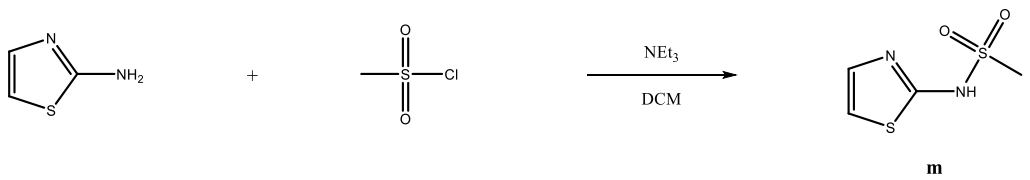

m

*Figure 39: Synthesis of Ligand **m**.*

A two-neck round bottom flask was charged with 45 mL dry DCM, 2-aminothiazole (1.00 g, 9.99 mmol, 1.00 eq.) and NEt_3 (25 mL, 20.5 mmol, 2.05 eq.). The flask was placed in an ice bath and methanesulfonyl chloride (9.30 mL, 12.0 mmol, 1.20 eq.) was added through a funnel over the course of two hours. After the complete addition of the methanesulfonyl chloride, the ice bath was removed, and the reaction mixture was stirred at r.t. overnight. The reaction was quenched with 100 mL 1N HCl and the organic layer was washed with brine (2 × 100 mL). The organic layer was dried over anhydrous sodium sulfate and the solvent was removed under reduced pressure. The orange viscous oil was purified by column chromatography (silica, gradient 4–8% MeOH in DCM). To remove the remaining DCM crystals, the solid was recrystallised in a small quantity of EtOAc to yield the ligand **m** as an orange solid (164 mg, 1.03 mmol, 10%).

^{1}H NMR (500 MHz, DMSO-d_6): 12.50 (s, 1H, NH), 7.24 (d, J = 4.7 Hz, 1H, CH-N), 6.80 (d, J = 4.7 Hz, 1H, CH-S), 2.88 (s, 3H, CH_3) ppm.

MS (ESI): Calculated for $C_4H_6N_2O_2S_2$ $[M + Na]^+$: 200.98; found: 200.94

3.3.9. 3-(4,4,5,5-tetramethyl-1,3,2-dioxaborolan-2-yl)benzenesulfonamide (**E3**):

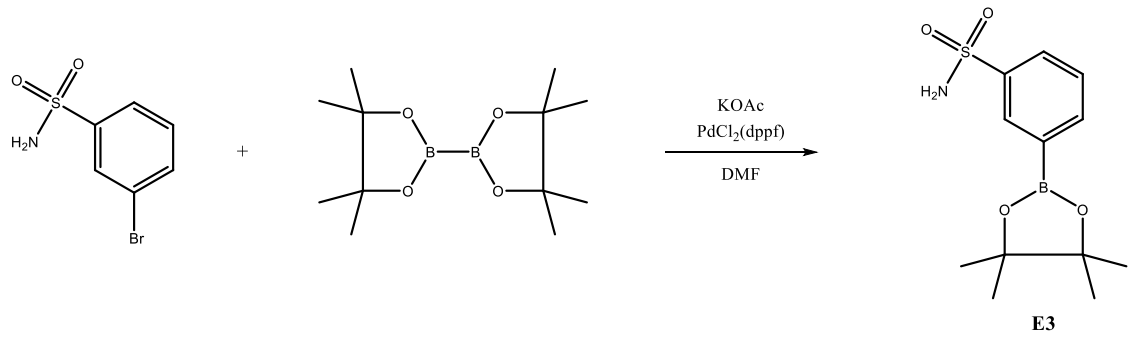

*Figure 40: Synthesis of compound **E3**.*

A two neck round bottom flask was charged with 40 mL dry DMF, 3-bromobenzene-1-sulfonamide (707 mg, 2.99 mmol, 1.00 eq.), bis(pinacole)diborane (800 mg, 3.15 mmol, 1.05 eq.) potassium acetate (883 mg, 8.99 mmol, 3.00 eq.) and [1,1´-Bis(diphenylphospino)ferrocene]-dichloropalladium(II) (123 mg, 0.17 mmol, 0.06 eq.). The reaction mixture was refluxed overnight at 90°C under argon atmosphere. The reaction was quenched with water (50 mL) and washed three times with ethyl acetate (60 mL). The combined organic layer was washed once again with brine and dried over anhydrous sodium sulfate. The solvent was removed under reduced pressure and the yellow viscous oil was purified by column chromatography (silica, gradient 30–40% ethyl acetate in *n*-hexane) to yield product **E3** as a colourless solid (493 mg, 1.73 mmol, 58%).

^{1}H-NMR (500 MHz, DMSO-d_6): δ 8.13 (s, 1H, CH: arom.), 7.92 (ddd, J = 7.9, 2.1, 1.2 Hz, 1H, CH: arom.), 7.86 – 7.83 (m, 1H, CH: arom.), 7.58 (dd, J = 7.6, 7.6 Hz, 1H, CH: arom.), 7.37 (s, 2H, NH_2), 1.31 (s, 12H, CH_3) ppm.

3.4. General complexation procedure

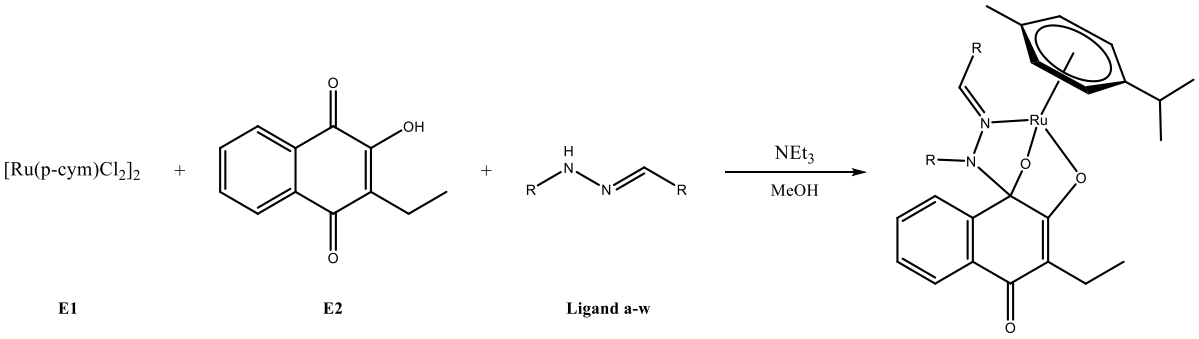

Figure 41: General procedure for complex synthesis.

Ruthenium dimer [Ru(*p*-cym)Cl_2]$_2$ (**E1**; 1.00 eq.), 2-hydroxy-3-ethylnaphthalene-1,4-dione (**E2**; 1.90 eq.) and the corresponding hydrazine ligand (1.90 eq.) were dissolved in 7–15 mL methanol. After stirring the reaction mixture for five minutes, triethylamine (6.00 eq.) was added, and the dark-red solution was heated to 60 °C under microwave irradiation for 15–20 minutes. The solvent was removed under reduced pressure and, if possible, the greenish to black crude product was purified by column chromatography.

3.4.1. [(3-Ethyl-1-(1H-κ*N*2-3-methylpyrazol-1-yl)-4-oxo-1,4-dihydronaphtalene-1,2-bis(olato)-κ*O*-κ*O*2)(η_6-*p*-cymene)ruthenium(II)] (**I**):

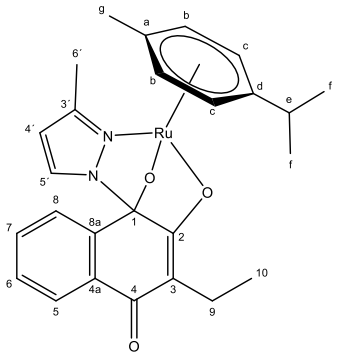

*Figure 42: Complex **I**.*

Following the general complexation procedure, [Ru(*p*-cym)Cl_2]$_2$ (75 mg, 0.12 mmol, 1.00 eq.), 2-hydroxy-3-ethylnaphthalene-1,4-dione (48 mg, 0.23 mmol, 1.95 eq.) and 3-methylpyrazole (19 µL, 0.23 mmol, 1.95 eq.) were dissolved in 10 mL methanol. After stirring the reaction mixture for 5 minutes, NEt_3 (54.5 µL, 0.73 mmol, 6.15 eq.) was added and the solution was heated to 60 °C under microwave irradiation for 20 minutes. The solvent was removed under reduced pressure and the crude red solid was purified by column chromatography (silica, 95% EtOAc + 5% NEt_3) to yield complex **I** as a yellow solid (50 mg, 0.10 mmol, 81%).

TLC (88:8:4 EtOAc:n-hexane:NEt_3): R_f = 0.55 (UV)

^{1}H-NMR (500.10 MHz, MeOD): δ 8.08 – 8.03 (m, 1H, CH: arom.), 7.59 – 7.52 (m, 3H, CH: arom.), 6.51 (d, J = 2.5 Hz, 1H, CH: 4´), 6.10 (d, J = 2.5 Hz, 1H, CH: 5´), 6.03 (d, J = 5.9 Hz, 1H, CH: c), 5.94 (d, J = 6.0 Hz, 1H, CH: c), 5.77 (d, J = 5.9 Hz, 1H, CH: b), 5.58 (d, J = 6.0 Hz, 1H, CH: b), 2.82 (hept, J = 7.1, 1H, CH: e), 2.63 (s, 3H, CH_3: 6´), 2.40 – 2.33 (m, 1H, CH_2: 9), 2.32 (s, 6H, CH_3: f), 2.29 – 2.21 (m, 1H, CH_2: g), 1.31 (m, 3H, CH_3: f), 0.88 – 0.84 (m, 3H, CH_3: 10) ppm.

^{13}C-NMR (600.25 MHz, MeOD): δ 183.7 (Cq: 2), 183.1 (Cq: 4), 140.6 (CH: 3´), 138.0 (Cq: arom.), 134.5 (Cq; arom.), 132.1 (CH: arom), 131.1 (CH: arom.), 127.8 (CH: 5´), 127.1 (CH: arom.), 127.0 (CH: arom.), 111.9 (Cq: 3), 108.8 (Cq: 4´), 108.7 (Cq: d) , 100.0 (Cq: d), 97.9 (Cq: 1), 83.4 (Cq: c), 82.9 (Cq; c), 80.0 (Cq; b), 79.8 (Cq; b), 32.7 (CH; e), 23.1 (Cq: f), 22.8 (Cq: f), 18.3 (CH_3: g), 16.9 (CH_2: 9), 13.7 (CH_3: 10), 11.2 (CH_3: 6´) ppm.

Elemental analysis Calculated for $C_{26}H_{28}N_2O_3Ru$: C 60.33%, H 5.45%, N 5.41%, O 9.27%. Found: C: 59.93%, H: 5.50%, N: 5.54%, O: 9.30%.

MS (ESI): Calculated for $C_{26}H_{28}N_2O_3Ru$ $[M + Na]^+$: 541.10; found: 541.14

3.4.2. [(3-Ethyl-1-(1H-κ*N*2-4-methylpyrazol-1-yl)-4-oxo-1,4-dihydronaphtalene-1, 2-bis(olato)-κ*O*1-κ*O*2)(η_6-*p*-cymene)ruthenium(II)] (**II**):

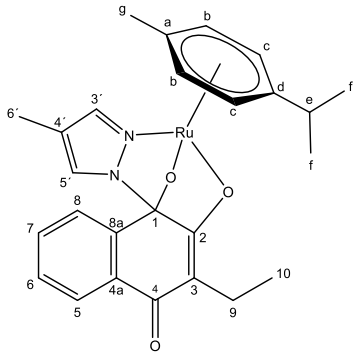

*Figure 43: Complex **II**.*

Following the general complexation procedure, [Ru(*p*-cym)Cl_2]$_2$ (101 mg, 0.16 mmol, 1.00 eq.), 2-hydroxy-3-ethylnaphthalene-1,4-dione (64.5 mg, 0.32 mmol, 2.00 eq.) and 4-methylpyrazole (25.7 µL, 0.31 mmol, 1.94 eq.) were dissolved in 7 mL methanol. After stirring the reaction mixture for 5 minutes, NEt_3 (136 µL, 0.98 mmol, 6.13 eq.) was added and the solution was heated to 60 °C under microwave irradiation for 20 minutes. The solvent was removed under reduced pressure and the crude red solid was purified by column chromatography (silica, 96% EtOAc + 4% NEt_3) to yield complex **II** as a yellow solid (82 mg, 0.13 mmol, 82%).

TLC (88:8:4 EtOAc:n-hexane:NEt_3): R_f = 0.55 (UV)

^{1}H-NMR (600.25 MHz, MeOD): δ 8.14 (s, 1H, CH: 3´), 8.10 – 8.06 (m, 1H, CH: arom.), 7.58 (m, 3H, 3 CH: arom.), 6.47 (s, 1H, CH: 5´), 5.93 (d, J = 5.2 Hz, 1H, CH: c), 5.84 (d, J = 5.4 Hz, 1H, CH: c), 5.58 (t, J = 5.4 Hz, 2H, 2 CH: b), 2.86 (hept., J = 6.9 Hz, 1H, CH: e), 2.37 (m, 1H, CH_2: 9), 2.32 (s, 3H, CH_3: g), 2.28 (m, 1H, CH_2: 9), 1.97 (s, 3H, CH: 6´), 1.33 (d, J = 6.9 Hz, 6H, 2 CH_3: f), 0.88 (t, J = 7.4 Hz, 3H, CH_3: 10) ppm.

^{13}C-NMR (600.25 MHz, MeOD): δ 183.7 (Cq: 2), 183.2 (Cq: 4), 141.3 (CH: 3´), 137.9 (Cq: arom.), 134.4 (Cq: arom.), 132.1 (CH: arom.), 131.1 (CH: arom), 127.7 (CH: 5´), 127.1 (CH: arom.), 126.9 (CH: arom.), 119.9 (Cq: 3), 112.2 (Cq: 4´), 101.2 (Cq: d), 98.4 (Cq: a), 94.6 (Cq: 1), 83.2 (Cq: c), 82.8 (Cq: c), 80.2 (Cq: b), 80.1 (Cq: b), 32.6 (CH: e), 23.1 (Cq; f), 22.8 (Cq: f), 18.4 (CH_3: g), 16.9 (CH_2: 9), 13.7 (CH_3: 10), 8.9 (CH_3: 6´) ppm.

Elemental analysis calculated for $C_{26}H_{28}N_2O_3Ru \cdot 0.5\ H_2O$: C 59.30%, H 5.55%, N 5.32%, O 10.63%. Found: C 59.07%, H 5.32% N 5.28%, O: 10.65%.

MS (ESI): calculated for $C_{26}H_{28}N_2O_2Ru$ $[M-H]^-$: 517.11; found: 517.11

3.4.3. [(3-Ethyl-1-(1H-κ*N*2-3,4-dimethylpyrazol-1-yl)-4-oxo-1,4-dihydronaphtalene-1,2-bis(olato)-κ*O*1-κ*O*2)(η_6-*p*-cymene)ruthenium(II)] (**III**):

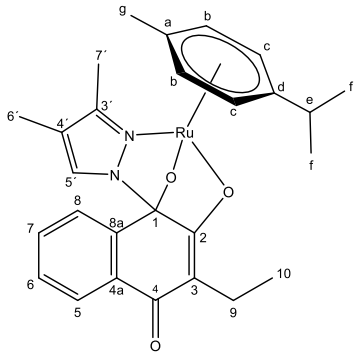

*Figure 44: Complex **III**.*

Following the general complexation procedure, $[Ru(p\text{-cym})Cl_2]_2$ (103 mg, 0.17 mmol, 1.00 eq.), 2-hydroxy-3-ethylnaphthalene-1,4-dione (63 mg, 0.31 mmol, 1.82 eq.) and 3,4-dimethylpyrazole (30 mg, 0.31 mmol, 1.82 eq.) were dissolved in 7 mL methanol. After stirring the reaction mixture for 5 minutes, NEt_3 (136 µL, 0.98 mmol, 5.76 eq.) was added and the solution was heated to 60 °C under microwave irradiation for 20 minutes. The solvent was removed under reduced pressure and the crude dark red solid was purified by column chromatography (silica, 95% EtOAc + 5% NEt_3) to yield complex **III** as a yellow solid (65 mg, 0.12 mmol, 72%).

TLC (88:8:4 EtOAc:n-hexane:NEt_3): R_f = 0.58 (UV)

^{1}H-NMR (500.10 MHz, MeOD): δ 8.10 – 8.06 (m, 1H, CH: arom.), 7.64 – 7.58 (m, 3H, CH: arom.), 6.37 (s, 1H, CH: 5´), 6.06 (d, J = 5.9 Hz, 1H, CH: c), 5.97 (d, J = 6.0 Hz, 1H, CH: c), 5.80 (d, J = 5.9 Hz, 1H, CH: b), 5.61 (d, J = 6.0 Hz, 1H, CH: b), 2.85 (hept, J = 7.2, 1H, CH: e), 2.58 (s, 1H, CH: 6´), 2.43 – 2.37 (m, 1H, CH: 9), 2.35 (s, 3H, CH_3: g), 2.36 – 2.25 (m, 1H, CH: 9), 1.9 (s, 3H, CH_3: 7´), 1.24 – 1.44 (m, 6H, CH_3: f), 0.90 (m, 3H, CH_3: 10) ppm.

^{13}C-NMR (600.25 MHz, MeOD): δ 184.6 (Cq: 2), 183.0 (Cq: 4), 140.6 (Cq: 3´), 138.1 (Cq: arom.), 134.5 (Cq: arom.), 132.1 (Cq: arom.), 131.1 (Cq: arom.), 127.8 (CH: 5´), 127.0 (Cq: arom.), 126.9 (Cq: arom.), 117.8 (Cq: 3), 111.9 (Cq: 4´), 99.8 (Cq: 1), 97.9 (Cq: a), 96.5 (Cq: d) 83.4 (Cq: c), 82.8 (Cq: c), 80.2 (Cq: b), 80.0 (Cq: b), 32.7 (CH: e), 23.1 (Cq: f), 22.8 (Cq: f), 18.3 (CH_3: g), 16.9 (Cq: 9), 13.7 (CH_3: 10), 12.5 (CH_3: 7´), 8.9 (CH_3: 6´) ppm.

Elemental analysis Calculated for $C_{26}H_{28}N_2O_3Ru \cdot 0.15\ H_2O$: C 60.69%, H 5.72%, N 5.24%, O 9.43%. Found: C 60.36%, H 5.56%, N: 5.45%, O: 9.43%.

MS (ESI): Calculated for $C_{27}H_{30}N_2O_3Ru$ $[M + Na]^+$:555.12; found: 555.16

3.4.4. [(3-Ethyl-1-(1H-κ*N*2-indazol-1-yl)-4-oxo-1,4-dihydronaphtalene-1,2-bis(olato)-κ*O*1-κ*O*2)(η_6-*p*-cymene)ruthenium(II)] (**IV**):

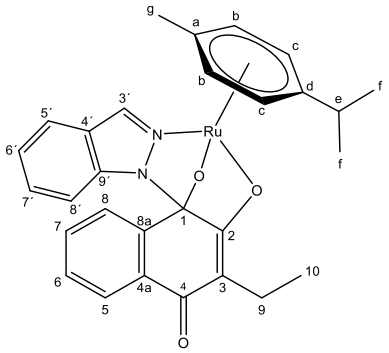

*Figure 45: Complex **IV**.*

Following the general complexation procedure, [Ru(*p*-cym)Cl_2]$_2$ (98 mg, 0.16 mmol, 1.00 eq.), 2-hydroxy-3-ethylnaphthalene-1,4-dione (63 mg, 0.31 mmol, 1.94 eq.) and indazole (36 mg, 0.30 mmol, 1.90 eq.) were dissolved in 7 mL methanol. After stirring the reaction mixture for 5 minutes, NEt_3 (137 µl, 0.99 mmol, 6.16 eq.) was added and the solution was heated to 60 °C under microwave irradiation for 20 minutes. The solvent was removed under reduced pressure and the crude red to black solid was purified by column chromatography (silica, 96% EtOAc + 4% NEt_3) to yield complex **IV** as a pale green solid (79 mg, 0.14 mmol, 89%).

TLC (93:3:4 EtOAc:*n*-hexane:NEt_3) R_f = 0.44 (UV)

^{1}H-NMR (600.25 MHz, MeOD): δ 8.99 (s, 1H), 8.20 (dd, J = 7.8, 1.4 Hz, 1H), 7.79 – 7.71 (m, 2H), 7.70 (ddd, J = 7.6, 7.6, 1.3 Hz, 1H), 7.60 (ddd, J = 7.5, 7.5, 1.4 Hz, 1H), 7.07 (dd, J = 7.5, 7.5 1H), 6.96 (dd, J = 7.9, 7.9 Hz 1H), 6.05 (d, J = 5.9 Hz, 1H), 5.94 (d, J = 5.9 Hz, 1H), 5.69 (d, J = 6.4 Hz, 2H), 5.37 (dd, J = 8.8, 0.9 Hz, 1H), 2.91 (hept., J = 6.9 Hz, 1H), 2.36 (s, 1H), 2.43 – 2.30 (m, 1H), 2.26 – 2.20 (m, 1H), 1.36 (dd, J = 6.9, 2.1 Hz, 6H), 0.82 (t, J = 7.4 Hz, 3H) ppm.

^{13}C-NMR (600 MHz, MeOD): δ 183.6 (Cq: 2), 183.2 (Cq: 4), 138.2 (Cq: 3´), 137.5 (Cq: arom.), 137.2 (Cq: arom.), 134.6 (Cq: arom.), 132.3 (Cq: arom.), 131.5 (Cq: arom.), 129.4 (Cq: arom.), 128.4 (Cq: arom.), 127.3 (Cq: arom.), 126.3 (Cq: arom.), 123.4 (Cq: arom.), 122.4 (Cq: 3´), 112.9 (Cq: 4´), 111.2 (Cq: 8´), 101.7 (Cq: d), 99.0 (Cq: a), 93.7 (Cq:1) 83.8 (Cq: c), 83.4 (Cq: c), 80.8 (Cq: b), 80.7 (Cq: b), 32.7 (CH: e), 23.1 (Cq: f), 22.8 (Cq: f), 18.3 (CH_3: g), 16.9 (CH_2: 9), 13.7 (CH3: 10) ppm.

Elemental analysis Calculated for $C_{26}H_{28}N_2O_3Ru \cdot 0.5\ H_2O$: C 61.97%, H 5.20%, N 4.98%, O 9.95%. Found: C 62.10%, H 5.34%, N 4.98%, O 9.95%.

MS (ESI): calculated for $C_{29}H_{28}N_2O_3Ru$ $[M+H]^+$: 555.12; found 555.12

4. Conclusion of the complexation experiments

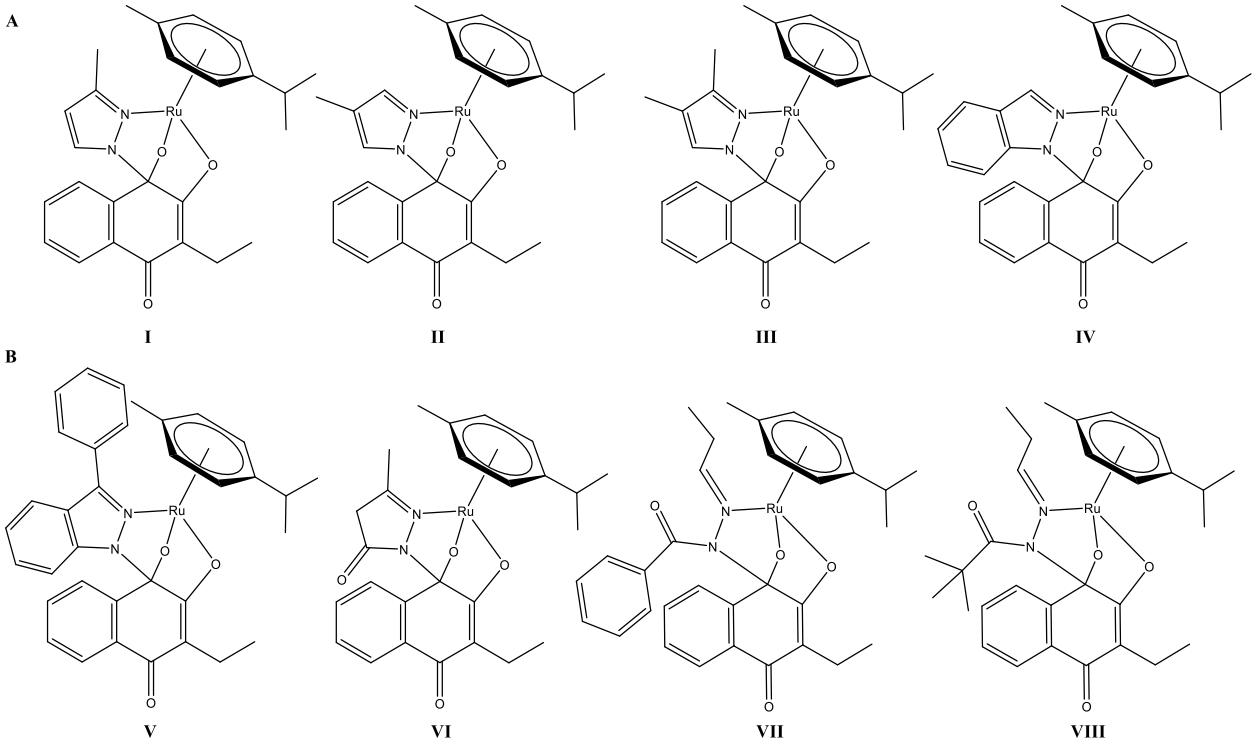

*Figure 46: A) Complexes **I–IV** were obtained in adequate purity.*
*B) The formation of complexes **V–VIII** was confirmed through ^{1}H and ^{13}C NMR spectroscopy.*

In conclusion, this thesis serves as a "proof of principle" to demonstrating that the 1,2-diazole moiety can be extended beyond the conventional pyrazole ligand for the formation of these novel tridentate ruthenium(II) arene complexes. Figure **46** presents all complexes which were successfully synthesized in the course of this study. Compounds **I–IV** were acquired in good yield with satisfying purity. Unfortunately, up to this day, all attempts to obtain purified complexes **VI-VIII** failed due to insufficient stability of these substances. This outcome suggests that the tridentate complexes containing an open-chain hydrazide moiety exhibit a less favorable structure compared to their pyrazolate analogues. Even though this class of ligands is reliant on the presence of an electron withdrawing group, the amide group incorporated in the complexes **VI–VIII** may be at least partially responsible for the instability of the compounds regarding purification by column chromatography and other methods. Complex **V** was stable under standard MPLC condition, yet no satisfying purity could be achieved. Furthermore, no complexes were formed with an open-chained ligands **s** and **t**, presumably due to steric hindrance of the benzyl group. Despite that, the steric demanding compound **h**, was able to form the tridentate motif. Additional research of the complexes **V**, **VII** and **VIII** would be beneficial for further clarification on the spatial orientation of these ligands.

5. Outlook

Since the methylated pyrazole complexes exhibited promising stability in organic solvents, the next apparent step for extended investigation would be to conduct UV/Vis stability measurements for the complexes **I–III** to determine their stability in aqueous media as well as assessing their redox properties *via* cyclic voltammetry. Moreover, the crystal structures of the complexes **I** and **III** would contribute to identifying the cause of the additional set of signals observed in their respective ^{1}H-NMR spectra.

Despite the complexation of hydrazide ligands being the main focus of this work, obtaining the complexes **VI–VII** in satisfying purity was not achievable. Additional purification setups beyond the methods attempted in this study (e.g., purification by column chromatography and precipitation) are necessary, should these complexes remain of interest for future research. Furthermore, in case the purified compounds demonstrate promising stability, the determination of their *in vitro* cytotoxicity is crucial in order to compare their anticancer potencies with the established parental complexes. Ultimately, conducting complexation experiments with non-cyclic bioactive ligands would be a feasible option to optimize the anticancer properties of this compound class by enabling interactions with different molecular targets.

Finally, due to the synthesis of the bioactive compound **i** being terminated because of to time restraints, complexation experiments with this potential ligand were not conducted. The implementation of alternative synthetic pathways may lead to a successful synthesis and purification of this molecule, enabling further research with this ligand.

6. References

[1] ABDULRIDHA M K, AL-MARZOQI A H, AL-AWSI G R L, 等. Anticancer Effects of Herbal Medicine Compounds and Novel Formulations: a Literature Review[J/OL]. Journal of Gastrointestinal Cancer, 2020, 51(3): 765-773. DOI:10.1007/s12029-020-00385-0.

[2] DEBELA D T, MUZAZU S G, HERARO K D, 等. New approaches and procedures for cancer treatment: Current perspectives[J/OL]. SAGE Open Medicine, 2021, 9: 20503121211034366. DOI:10.1177/20503121211034366.

[3] HATTON I A, GALBRAITH E D, MERLEAU N S C, 等. The human cell count and size distribution[J/OL]. Proceedings of the National Academy of Sciences, 2023, 120(39): e2303077120. DOI:10.1073/pnas.2303077120.

[4] NOWELL P C. The clonal evolution of tumor cell populations[J/OL]. Science (New York, N.Y.), 1976, 194(4260): 23-28. DOI:10.1126/science.959840.

[5] ALBERTS B, JOHNSON A, LEWIS J, 等. Molecular Biology of the Cell[M]. 6 版. New York, NY: Garland Science, 2014.

[6] FARES J, FARES M Y, KHACHFE H H, 等. Molecular principles of metastasis: a hallmark of cancer revisited[J/OL]. Signal Transduction and Targeted Therapy, 2020, 5(1): 1-17. DOI:10.1038/s41392-020-0134-x.

[7] What is cancer?[EB/OL]. [2023-10-17]. https://www.cancer.org.au/cancer-information/what-is-cancer.

[8] COOPER G M, COOPER G M. The Cell[M]. 2nd 版. Sinauer Associates, 2000.

[9] HANAHAN D, WEINBERG R A. The Hallmarks of Cancer[J/OL]. Cell, 2000, 100(1): 57-70. DOI:10.1016/S0092-8674(00)81683-9.

[10] HANAHAN D. Hallmarks of Cancer: New Dimensions[J/OL]. Cancer Discovery, 2022, 12(1): 31-46. DOI:10.1158/2159-8290.CD-21-1059.

[11] PECORINO L, PECORINO L. Molecular Biology of Cancer: Mechanisms, Targets, and Therapeutics[M]. Fifth Edition, Fifth Edition. Oxford, New York: Oxford University Press, 2021.

[12] AMIN A R M R, KARPOWICZ P A, CAREY T E, 等. Evasion of anti-growth signaling: a key step in tumorigenesis and potential target for treatment and prophylaxis by natural

compounds[J/OL]. Seminars in cancer biology, 2015, 35 Suppl: S55-S77. DOI:10.1016/j.semcancer.2015.02.005.

[13] SCHEEL C H, SCHÄFER R. Editorial: Hallmark of cancer: Evasion of growth suppressors[J/OL]. Frontiers in Oncology, 2023, 13: 1170115. DOI:10.3389/fonc.2023.1170115.

[14] ZHANG Y, CAO L, NGUYEN D, 等. TP53 mutations in epithelial ovarian cancer[J/OL]. Translational Cancer Research, 2016, 5(6): 650-663. DOI:10.21037/tcr.2016.08.40.

[15] NEOPHYTOU C M, KYRIAKOU T C, PAPAGEORGIS P. Mechanisms of Metastatic Tumor Dormancy and Implications for Cancer Therapy[J/OL]. International Journal of Molecular Sciences, 2019, 20(24): 6158. DOI:10.3390/ijms20246158.

[16] STEEG P S. Tumor metastasis: mechanistic insights and clinical challenges[J/OL]. Nature Medicine, 2006, 12(8): 895-904. DOI:10.1038/nm1469.

[17] CAJA L, TAN E J. Epithelium to Mesenchyme Transition[M/OL]//BOFFETTA P, HAINAUT P. Encyclopedia of Cancer (Third Edition). Oxford: Academic Press, 2019: 14-23[2023-11-09]. https://www.sciencedirect.com/science/article/pii/B9780128012383650249. DOI:10.1016/B978-0-12-801238-3.65024-9.

[18] PAGET S. THE DISTRIBUTION OF SECONDARY GROWTHS IN CANCER OF THE BREAST.[J/OL]. The Lancet, 1889, 133(3421): 571-573. DOI:10.1016/S0140-6736(00)49915-0.

[19] TALMADGE J E, FIDLER I J. AACR centennial series: the biology of cancer metastasis: historical perspective[J/OL]. Cancer Research, 2010, 70(14): 5649-5669. DOI:10.1158/0008-5472.CAN-10-1040.

[20] MASSAGUÉ J, OBENAUF A C. Metastatic colonization by circulating tumour cells[J/OL]. Nature, 2016, 529(7586): 298-306. DOI:10.1038/nature17038.

[21] HANAHAN D, WEINBERG R A. Hallmarks of Cancer: The Next Generation[J/OL]. Cell, 2011, 144(5): 646-674. DOI:10.1016/j.cell.2011.02.013.

[22] GARCÍA-CHICO C, LÓPEZ-ORTIZ S, PEÑÍN-GRANDES S, 等. Physical Exercise and the Hallmarks of Breast Cancer: A Narrative Review[J/OL]. Cancers, 2023, 15(1): 324. DOI:10.3390/cancers15010324.

[23] RIBATTI D. Angiogenesis[M/OL]//MALOY S, HUGHES K. Brenner's Encyclopedia of Genetics (Second Edition). San Diego: Academic Press, 2013: 130-132[2023-11-07]. https://www.sciencedirect.com/science/article/pii/B9780123749840000656. DOI:10.1016/B978-0-12-374984-0.00065-6.

[24] LODISH H F, BERK A, KAISER C, 等. Molecular cell biology[M]. Eighth edition. New York: W.H. Freeman-Macmillan Learning, 2016.

[25] BACKER M V, BACKER J M. Imaging Key Biomarkers of Tumor Angiogenesis[J/OL]. Theranostics, 2012, 2(5): 502-515. DOI:10.7150/thno.3623.

[26] JAN R, CHAUDHRY G e S. Understanding Apoptosis and Apoptotic Pathways Targeted Cancer Therapeutics[J/OL]. Advanced Pharmaceutical Bulletin, 2019, 9(2): 205-218. DOI:10.15171/apb.2019.024.

[27] SUMNER C. Hallmarks of Cancer: Resisting Cell Death[EB/OL]. [2023-11-10]. https://blog.cellsignal.com/hallmarks-of-cancer-resisting-cell-death.

[28] FULDA S. Evasion of Apoptosis as a Cellular Stress Response in Cancer[J/OL]. International Journal of Cell Biology, 2010, 2010: e370835. DOI:10.1155/2010/370835.

[29] VINAY D S, RYAN E P, PAWELEC G, 等. Immune evasion in cancer: Mechanistic basis and therapeutic strategies[J/OL]. Seminars in Cancer Biology, 2015, 35: S185-S198. DOI:10.1016/j.semcancer.2015.03.004.

[30] PAHWA R, GOYAL A, JIALAL I. Chronic Inflammation[M/OL]//StatPearls. Treasure Island (FL): StatPearls Publishing, 2023[2023-11-13]. http://www.ncbi.nlm.nih.gov/books/NBK493173/.

[31] DE LARCO J E, WUERTZ B R K, FURCHT L T. The Potential Role of Neutrophils in Promoting the Metastatic Phenotype of Tumors Releasing Interleukin-8[J/OL]. Clinical Cancer Research, 2004, 10(15): 4895-4900. DOI:10.1158/1078-0432.CCR-03-0760.

[32] ROBINSON J M. Reactive oxygen species in phagocytic leukocytes[J/OL]. Histochemistry and Cell Biology, 2008, 130(2): 281. DOI:10.1007/s00418-008-0461-4.

[33] YAO Y, DAI W. Genomic Instability and Cancer[J/OL]. Journal of carcinogenesis & mutagenesis, 2014, 5: 1000165. DOI:10.4172/2157-2518.1000165.

[34] NEGRINI S, GORGOULIS V G, HALAZONETIS T D. Genomic instability--an evolving hallmark of cancer[J/OL]. Nature Reviews. Molecular Cell Biology, 2010, 11(3): 220-228. DOI:10.1038/nrm2858.

[35] LIBERTI M V, LOCASALE J W. The Warburg Effect: How Does it Benefit Cancer Cells?[J/OL]. Trends in biochemical sciences, 2016, 41(3): 211-218. DOI:10.1016/j.tibs.2015.12.001.

[36] DATTANI S, SPOONER F, RITCHIE H, 等. Causes of Death[J/OL]. Our World in Data, 2023[2023-10-18]. https://ourworldindata.org/causes-of-death.

[37] DYBA T, RANDI G, BRAY F, 等. The European cancer burden in 2020: Incidence and mortality estimates for 40 countries and 25 major cancers[J/OL]. European Journal of Cancer, 2021, 157: 308-347. DOI:10.1016/j.ejca.2021.07.039.

[38] Cancer cases and deaths on the rise in the EU[EB/OL]. (2023-05-17)[2023-10-17]. https://joint-research-centre.ec.europa.eu/jrc-news-and-updates/cancer-cases-and-deaths-rise-eu-2023-10-02_en.

[39] Europe[EB/OL]//The Cancer Atlas. [2023-11-14]. http://canceratlas.cancer.org/F5S.

[40] Cancer in Europe: 5 things the data tells us[EB/OL]. [2023-12-11]. https://joint-research-centre.ec.europa.eu/jrc-news-and-updates/cancer-europe-5-things-data-tells-us-2022-01-13_en.

[41] 908-europe-fact-sheets.pdf[Z/OL]. [2023-10-16]. https://gco.iarc.fr/today/data/factsheets/populations/908-europe-fact-sheets.pdf.

[42] FISHER B, WOLMARK N. The Current Status of Systemic Adjuvant Therapy in the Management of Primary Breast Cancer[J/OL]. Surgical Clinics of North America, 1981, 61(6): 1347-1360. DOI:10.1016/S0039-6109(16)42589-2.

[43] HALSTED W S. I. The Results of Operations for the Cure of Cancer of the Breast Performed at the Johns Hopkins Hospital from June, 1889, to January, 1894[J]. Annals of Surgery, 1894, 20(5): 497-555.

[44] SCHIRRMACHER V. From chemotherapy to biological therapy: A review of novel concepts to reduce the side effects of systemic cancer treatment (Review)[J/OL]. International Journal of Oncology, 2018, 54(2): 407-419. DOI:10.3892/ijo.2018.4661.

[45] MCALEER S. A history of cancer and its treatment[J]. The Ulster Medical Journal, 2022, 91(3): 124-129.

[46] BASKAR R, LEE K A, YEO R, 等. Cancer and Radiation Therapy: Current Advances and Future Directions[J/OL]. International Journal of Medical Sciences, 2012, 9(3): 193-199. DOI:10.7150/ijms.3635.

[47] PALUMBO M O, KAVAN P, MILLER W H, 等. Systemic cancer therapy: achievements and challenges that lie ahead[J/OL]. Frontiers in Pharmacology, 2013, 4: 57. DOI:10.3389/fphar.2013.00057.

[48] EINHORN L H, DONOHUE J. Cis-diamminedichloroplatinum, vinblastine, and bleomycin combination chemotherapy in disseminated testicular cancer[J/OL]. Annals of Internal Medicine, 1977, 87(3): 293-298. DOI:10.7326/0003-4819-87-3-293.

[49] GROESSL M, TSYBIN Y O, HARTINGER C G, 等. Ruthenium versus Platinum: Interactions of Anticancer Metallodrugs with Duplex Oligonucleotides Characterised by Electrospray Ionisation-Mass Spectrometry[J/OL]. Journal of biological inorganic chemistry : JBIC : a publication of the Society of Biological Inorganic Chemistry, 2010, 15(5): 677-688. DOI:10.1007/s00775-010-0635-0.

[50] ZHANG C, XU C, GAO X, 等. Platinum-based drugs for cancer therapy and anti-tumor strategies[J/OL]. Theranostics, 2022, 12(5): 2115-2132. DOI:10.7150/thno.69424.

[51] KELLAND L. The resurgence of platinum-based cancer chemotherapy[J/OL]. Nature Reviews. Cancer, 2007, 7(8): 573-584. DOI:10.1038/nrc2167.

[52] CHAVAIN N, BIOT C. Organometallic complexes: new tools for chemotherapy[J/OL]. Current Medicinal Chemistry, 2010, 17(25): 2729-2745. DOI:10.2174/092986710791859306.

[53] ASTOLFI L, GHISELLI S, GUARAN V, 等. Correlation of adverse effects of cisplatin administration in patients affected by solid tumours: A retrospective evaluation[J/OL]. Oncology Reports, 2013, 29(4): 1285-1292. DOI:10.3892/or.2013.2279.

[54] GASSER G, OTT I, METZLER-NOLTE N. Organometallic Anticancer Compounds[J/OL]. Journal of Medicinal Chemistry, 2011, 54(1): 3-25. DOI:10.1021/jm100020w.

[55] KANG B W, KIM J G, KWON O K, 等. Non-platinum-based chemotherapy for treatment of advanced gastric cancer: 5-fluorouracil, taxanes, and irinotecan[J/OL]. World Journal of Gastroenterology : WJG, 2014, 20(18): 5396-5402. DOI:10.3748/wjg.v20.i18.5396.

[56] FERRARO M G, PICCOLO M, MISSO G, 等. Bioactivity and Development of Small Non-Platinum Metal-Based Chemotherapeutics[J/OL]. Pharmaceutics, 2022, 14(5): 954. DOI:10.3390/pharmaceutics14050954.

[57] PENG K, ZHENG Y, XIA W, 等. Organometallic anti-tumor agents: targeting from biomolecules to dynamic bioprocesses[J/OL]. Chemical Society Reviews, 2023, 52(8): 2790-2832. DOI:10.1039/D2CS00757F.

[58] CINI M, BRADSHAW T D, WOODWARD S. Using titanium complexes to defeat cancer: the view from the shoulders of titans[J/OL]. Chemical Society Reviews, 2017, 46(4): 1040-1051. DOI:10.1039/C6CS00860G.

[59] YEO C I, OOI K K, TIEKINK E R T. Gold-Based Medicine: A Paradigm Shift in Anti-Cancer Therapy?[J/OL]. Molecules : A Journal of Synthetic Chemistry and Natural Product Chemistry, 2018, 23(6): 1410. DOI:10.3390/molecules23061410.

[60] MORENO-ALCÁNTAR G, PICCHETTI P, CASINI A. Gold Complexes in Anticancer Therapy: From New Design Principles to Particle-Based Delivery Systems[J/OL]. Angewandte Chemie International Edition, 2023, 62(22): e202218000. DOI:10.1002/anie.202218000.

[61] GELDMACHER Y, OLESZAK M, SHELDRICK W S. Rhodium(III) and iridium(III) complexes as anticancer agents[J/OL]. Inorganica Chimica Acta, 2012, 393: 84-102. DOI:10.1016/j.ica.2012.06.046.

[62] MA D L, WU C, WU K J, 等. Iridium(III) Complexes Targeting Apoptotic Cell Death in Cancer Cells[J/OL]. Molecules, 2019, 24(15)[2023-11-21]. https://www.ncbi.nlm.nih.gov/pmc/articles/PMC6696146/. DOI:10.3390/molecules24152739.

[63] YANG T, ZHU M, JIANG M, 等. Current status of iridium-based complexes against lung cancer[J/OL]. Frontiers in Pharmacology, 2022, 13[2023-11-21]. https://www.frontiersin.org/articles/10.3389/fphar.2022.1025544.

[64] THOMAS S J, BALÓNOVÁ B, CINATL JR. J, 等. Thiourea and Guanidine Compounds and Their Iridium Complexes in Drug-Resistant Cancer Cell Lines: Structure-Activity Relationships and Direct Luminescent Imaging[J/OL]. ChemMedChem, 2020, 15(4): 349-353. DOI:10.1002/cmdc.201900591.

[65] SHARMA S A, P S, ROY N, 等. Advances in novel iridium (III) based complexes for anticancer applications: A review[J/OL]. Inorganica Chimica Acta, 2020, 513: 119925. DOI:10.1016/j.ica.2020.119925.

[66] YE R R, CAO J J, TAN C P, 等. Valproic Acid-Functionalized Cyclometalated Iridium(III) Complexes as Mitochondria-Targeting Anticancer Agents[J/OL]. Chemistry – A European Journal, 2017, 23(60): 15166-15176. DOI:10.1002/chem.201703157.

[67] BASHIR M, MANTOO I A, ARJMAND F, 等. An overview of advancement of organoruthenium(II) complexes as prospective anticancer agents[J/OL]. Coordination Chemistry Reviews, 2023, 487: 215169. DOI:10.1016/j.ccr.2023.215169.

[68] AITKEN J B, ANTONY S, WEEKLEY C M, 等. Distinct cellular fates for KP1019 and NAMI-A determined by X-ray fluorescence imaging of single cells†[J/OL]. Metallomics, 2012, 4(10): 1051-1056. DOI:10.1039/c2mt20072d.

[69] TRONDL R, HEFFETER P, KOWOL C R, 等. NKP-1339, the first ruthenium-based anticancer drug on the edge to clinical application[J/OL]. Chemical Science, 2014, 5(8): 2925-2932. DOI:10.1039/C3SC53243G.

[70] VACCA A, BRUNO M, BOCCARELLI A, 等. Inhibition of endothelial cell functions and of angiogenesis by the metastasis inhibitor NAMI-A[J/OL]. British Journal of Cancer, 2002, 86(6): 993-998. DOI:10.1038/sj.bjc.6600176.

[71] HARTINGER C G, JAKUPEC M A, ZORBAS-SEIFRIED S, 等. KP1019, A New Redox-Active Anticancer Agent – Preclinical Development and Results of a Clinical Phase I Study in Tumor Patients[J/OL]. Chemistry & Biodiversity, 2008, 5(10): 2140-2155. DOI:10.1002/cbdv.200890195.

[72] ALESSIO E, MESSORI L. NAMI-A and KP1019/1339, Two Iconic Ruthenium Anticancer Drug Candidates Face-to-Face: A Case Story in Medicinal Inorganic Chemistry[J/OL]. Molecules (Basel, Switzerland), 2019, 24(10): 1995. DOI:10.3390/molecules24101995.

[73] BOLD THERAPEUTICS, INC. A Phase 1b/2a Dose Escalation Study of BOLD-100 in Combination With FOLFOX Chemotherapy in Patients With Advanced Solid Tumours: NCT04421820[R/OL]. clinicaltrials.gov, 2023[2023-01-01]. https://clinicaltrials.gov/study/NCT04421820.

[74] SPRATLIN J L, O´KANE G, GOODWIN R A, 等. BOLD-100-001 (TRIO039): A phase 1b dose-escalation study of BOLD-100 in combination with FOLFOX chemotherapy in patients with advanced gastrointestinal solid cancers: Interim safety, tolerability, and efficacy.[J/OL]. Journal of Clinical Oncology, 2022, 40(16_suppl): 3031-3031. DOI:10.1200/JCO.2022.40.16_suppl.3031.

[75] BAKEWELL S, CONDE I, FALLAH Y, 等. Inhibition of DNA Repair Pathways and Induction of ROS Are Potential Mechanisms of Action of the Small Molecule Inhibitor BOLD-100 in Breast Cancer[J/OL]. Cancers, 2020, 12(9): 2647. DOI:10.3390/cancers12092647.

[76] EHRLICH P, BERTHEIM A. Über das salzsaure 3.3′-Diamino-4.4′-dioxy-arsenobenzol und seine nächsten Verwandten[J/OL]. Berichte der deutschen chemischen Gesellschaft, 1912, 45(1): 756-766. DOI:10.1002/cber.191204501110.

[77] GASSER G, METZLER-NOLTE N. The potential of organometallic complexes in medicinal chemistry[J/OL]. Current Opinion in Chemical Biology, 2012, 16(1-2): 84-91. DOI:10.1016/j.cbpa.2012.01.013.

[78] FREZZA M, HINDO S, CHEN D, 等. Novel Metals and Metal Complexes as Platforms for Cancer Therapy[J]. Current pharmaceutical design, 2010, 16(16): 1813-1825.

[79] KUMAR P, GUPTA R K, PANDEY D S. Half-sandwich arene ruthenium complexes: synthetic strategies and relevance in catalysis[J/OL]. Chemical Society Reviews, 2013, 43(2): 707-733. DOI:10.1039/C3CS60189G.

[80] SWAMINATHAN S, HARIBABU J, BALAKRISHNAN N, 等. Piano stool Ru(II)-arene complexes having three monodentate legs: A comprehensive review on their development as anticancer therapeutics over the past decade[J/OL]. Coordination Chemistry Reviews, 2022, 459: 214403. DOI:10.1016/j.ccr.2021.214403.

[81] SCOLARO C, HARTINGER C G, ALLARDYCE C S, 等. Hydrolysis study of the bifunctional antitumour compound RAPTA-C, [Ru(eta6-p-cymene)Cl2(pta)][J/OL]. Journal of Inorganic Biochemistry, 2008, 102(9): 1743-1748. DOI:10.1016/j.jinorgbio.2008.05.004.

[82] ASTARINA A, CHOW M J, ANG W H. Transcription Inhibition by Organometallic Ruthenium–Arene Anticancer Complexes in Live Mammalian Cells[J/OL]. Australian Journal of Chemistry, 2012, 65(9): 1271-1276. DOI:10.1071/CH12059.

[83] GEISLER H, WERNITZNIG D, HEJL M, 等. Novel phthiocol-based organometallics with tridentate coordination motif and their unexpected cytotoxic behaviour[J/OL]. Dalton Transactions, 2020, 49(5): 1393-1397. DOI:10.1039/C9DT04462K.

[84] BRAIBANTI A, DALLAVALLE F, MORI G, 等. Thermodynamic evaluation of chelate and cooperativity effects[J/OL]. Inorganica Chimica Acta, 1983, 79: 91-92. DOI:10.1016/S0020-1693(00)95124-7.

[85] CSEH K, GEISLER H, STANOJKOVSKA K, 等. Arene Variation of Highly Cytotoxic Tridentate Naphthoquinone-Based Ruthenium(II) Complexes and In-Depth In Vitro Studies[J/OL]. Pharmaceutics, 2022, 14(11): 2466. DOI:10.3390/pharmaceutics14112466.

[86] GEISLER H, WESTERMAYR J, CSEH K, 等. Tridentate 3-Substituted Naphthoquinone Ruthenium Arene Complexes: Synthesis, Characterization, Aqueous Behavior, and Theoretical and Biological Studies[J/OL]. Inorganic Chemistry, 2021, 60(13): 9805-9819. DOI:10.1021/acs.inorgchem.1c01083.

[87] RENFREW A K. Transition metal complexes with bioactive ligands: mechanisms for selective ligand release and applications for drug delivery[J/OL]. Metallomics, 2014, 6(8): 1324-1335. DOI:10.1039/C4MT00069B.

[88] SUN D, GAO W, HU H, 等. Why 90% of clinical drug development fails and how to improve it?[J/OL]. Acta Pharmaceutica Sinica. B, 2022, 12(7): 3049-3062. DOI:10.1016/j.apsb.2022.02.002.

[89] HODGSON J. ADMET—turning chemicals into drugs[J/OL]. Nature Biotechnology, 2001, 19(8): 722-726. DOI:10.1038/90761.

[90] TALEVI A. Multi-target pharmacology: possibilities and limitations of the “skeleton key approach” from a medicinal chemist perspective[J/OL]. Frontiers in Pharmacology, 2015, 6[2023-12-04]. https://www.frontiersin.org/articles/10.3389/fphar.2015.00205.

[91] AMININ D, POLONIK S. 1,4-Naphthoquinones: Some Biological Properties and Application[J/OL]. Chemical & Pharmaceutical Bulletin, 2020, 68(1): 46-57. DOI:10.1248/cpb.c19-00911.

[92] PEREYRA C E, DANTAS R F, FERREIRA S B, 等. The diverse mechanisms and anticancer potential of naphthoquinones[J/OL]. Cancer Cell International, 2019, 19(1): 207. DOI:10.1186/s12935-019-0925-8.

[93] DURÁN A G, CHINCHILLA N, SIMONET A M, 等. Biological Activity of Naphthoquinones Derivatives in the Search of Anticancer Lead Compounds[J/OL]. Toxins, 2023, 15(5): 348. DOI:10.3390/toxins15050348.

[94] NQO1 NAD(P)H quinone dehydrogenase 1 [Homo sapiens (human)] - Gene - NCBI[EB/OL]. [2023-11-22]. https://www.ncbi.nlm.nih.gov/gene/1728.

[95] PIDUGU L S M, MBIMBA J C E, AHMAD M, 等. A direct interaction between NQO1 and a chemotherapeutic dimeric naphthoquinone[J/OL]. BMC Structural Biology, 2016, 16[2023-11-23]. https://www.ncbi.nlm.nih.gov/pmc/articles/PMC4730606/. DOI:10.1186/s12900-016-0052-x.

[96] KARROUCHI K, RADI S, RAMLI Y, 等. Synthesis and Pharmacological Activities of Pyrazole Derivatives: A Review[J/OL]. Molecules : A Journal of Synthetic Chemistry and Natural Product Chemistry, 2018, 23(1): 134. DOI:10.3390/molecules23010134.

[97] LIN W S, KUWATA S. Recent Developments in Reactions and Catalysis of Protic Pyrazole Complexes[J/OL]. Molecules, 2023, 28(8): 3529. DOI:10.3390/molecules28083529.

[98] AZIZ H, ZAHOOR A F, AHMAD S, 等. PYRAZOLE BEARING MOLECULES AS BIOACTIVE SCAFFOLDS: A REVIEW[J/OL]. Journal of the Chilean Chemical Society, 2020, 65(1): 4746-4753. DOI:10.4067/S0717-97072020000104746.

[99] STOLLER J L, HOLUBITSKY I B, HARRISON R C, 等. Complications of the histalog test of gastric acid secretion[J/OL]. The American Journal of Digestive Diseases, 1970, 15(7): 647-651. DOI:10.1007/BF02236024.

[100] BENNANI F E, DOUDACH L, CHERRAH Y, 等. Overview of recent developments of pyrazole derivatives as an anticancer agent in different cell line[J/OL]. Bioorganic Chemistry, 2020, 97: 103470. DOI:10.1016/j.bioorg.2019.103470.

[101] ZHENG L, CHEN Z, KAWAKAMI M, 等. Tyrosine Threonine Kinase Inhibition Eliminates Lung Cancers by Augmenting Apoptosis and Polyploidy[J/OL]. Molecular Cancer Therapeutics, 2019, 18(10): 1775-1786. DOI:10.1158/1535-7163.MCT-18-0864.

[102] LAUFER R, NG G, LIU Y, 等. Discovery of inhibitors of the mitotic kinase TTK based on N-(3-(3-sulfamoylphenyl)-1H-indazol-5-yl)-acetamides and carboxamides[J/OL]. Bioorganic & Medicinal Chemistry, 2014, 22(17): 4968-4997. DOI:10.1016/j.bmc.2014.06.027.

[103] SWEENEY M J, DAVIS F A, GUTOWSKI G E, 等. Experimental Antitumor Activity of Pyrazomycin1[J]. Cancer Research, 1973, 33(11): 2619-2623.

[104] SANTOS N E, CARREIRA A R F, SILVA V L M, 等. Natural and Biomimetic Antitumor Pyrazoles, A Perspective[J/OL]. Molecules, 2020, 25(6): 1364. DOI:10.3390/molecules25061364.

[105] HALCROW M A. Pyrazoles and pyrazolides-flexible synthons in self-assembly[J/OL]. Dalton Transactions (Cambridge, England: 2003), 2009(12): 2059-2073. DOI:10.1039/b815577a.

[106] POPIOŁEK Ł. Hydrazide–hydrazones as potential antimicrobial agents: overview of the literature since 2010[J/OL]. Medicinal Chemistry Research, 2017, 26(2): 287-301. DOI:10.1007/s00044-016-1756-y.

[107] THOTA S, RODRIGUES D A, PINHEIRO P de S M, 等. N-Acylhydrazones as drugs[J/OL]. Bioorganic & Medicinal Chemistry Letters, 2018, 28(17): 2797-2806. DOI:10.1016/j.bmcl.2018.07.015.

[108] LIMA P C, LIMA L M, DA SILVA K C M, 等. Synthesis and analgesic activity of novel N-acylarylhydrazones and isosters, derived from natural safrole##This paper represents contribution # 36 of the LASSBio, UFRJ (Br.) (LASSBio, http://acd.ufrj.br/≈pharma/lassbio); For

contribution # 35, see [24].[J/OL]. European Journal of Medicinal Chemistry, 2000, 35(2): 187-203. DOI:10.1016/S0223-5234(00)00120-3.

[109] SOCEA L I, BARBUCEANU S F, PAHONTU E M, 等. Acylhydrazones and Their Biological Activity: A Review[J/OL]. Molecules (Basel, Switzerland), 2022, 27(24): 8719. DOI:10.3390/molecules27248719.

[110] POLO-CERÓN D, HINCAPIÉ-OTERO M M, JOAQUI-JOAQUI A. Synthesis and characterization of four N-acylhydrazones as potential O,N,O donors for Cu2+: An experimental and theoretical study[J/OL]. Universitas Scientiarum, 2021, 26(2): 193-215. DOI:10.11144/Javeriana.SC26-2.saco.

[111] MORGAN C W, JULIEN O, UNGER E K, 等. Chapter Eight - Turning ON Caspases with Genetics and Small Molecules[M/OL]//ASHKENAZI A, YUAN J, WELLS J A. Methods in Enzymology: 卷 544. Academic Press, 2014: 179-213[2023-12-06]. https://www.sciencedirect.com/science/article/pii/B978012417158900008X. DOI:10.1016/B978-0-12-417158-9.00008-X.

[112] DANCIU O. (STM-03) Phase I Study of Procaspase Activating Compound-1 (PAC-1) in the Treatment of Advanced Malignancies - Component 1: NCT02355535[R/OL]. clinicaltrials.gov, 2020[2023-01-01]. https://clinicaltrials.gov/study/NCT02355535.

[113] DANCIU O C, HOLDHOFF M, PETERSON R A, 等. Phase I study of procaspase-activating compound-1 (PAC-1) in the treatment of advanced malignancies[J/OL]. British Journal of Cancer, 2023, 128(5): 783-792. DOI:10.1038/s41416-022-02089-7.

[114] PATEL P R, HENDERSON S H, ROE M S, 等. Decarboxylative Bromination of Heteroarenes: Initial Mechanistic Insights[J/OL]. Synlett, 2020, 31(16): 1603-1607. DOI:10.1055/s-0040-1707901.

[115] YOUNGSAYE W, HARTLAND C L, MORGAN B J, 等. ML212: A small-molecule probe for investigating fluconazole resistance mechanisms in *Candida albicans*[J/OL]. Beilstein Journal of Organic Chemistry, 2013, 9: 1501-1507. DOI:10.3762/bjoc.9.171.

[116] WU F, ZHU K, WU G, 等. Nickel-Catalyzed C-O Cross-Coupling Reaction at Low Catalytic Loading with Weak Base Participation[J/OL]. European Journal of Organic Chemistry, 2020, 2020(4): 519-522. DOI:10.1002/ejoc.201901851.

[117] CROFT T S, MCBRADY J J. Fluoroalkylthio five-membered heteroaromatics[J/OL]. Journal of Heterocyclic Chemistry, 1975, 12(5): 845-849. DOI:10.1002/jhet.5570120507.

[118] KALITA S J, BAYAN R, DEVI J, 等. A new, convenient and expeditious synthesis of 4-alkyl-5-methyl-1H-pyrazol-3-ols in water through a multicomponent reaction[J/OL]. Tetrahedron Letters, 2017, 58(6): 566-569. DOI:10.1016/j.tetlet.2016.12.084.

[119] HAASNOOT J G. Mononuclear, oligonuclear and polynuclear metal coordination compounds with 1,2,4-triazole derivatives as ligands[J/OL]. Coordination Chemistry Reviews, 2000, 200-202: 131-185. DOI:10.1016/S0010-8545(00)00266-6.

[120] PANNE P, FOX J M. Rh-Catalyzed Intermolecular Reactions of Alkynes with α-Diazoesters That Possess β-Hydrogens: Ligand-Based Control over Divergent Pathways[J/OL]. Journal of the American Chemical Society, 2007, 129(1): 22-23. DOI:10.1021/ja0660195.

[121] KANDIOLLER W, HARTINGER C G, NAZAROV A A, 等. Maltol-derived ruthenium-cymene complexes with tumor inhibiting properties: the impact of ligand-metal bond stability on anticancer activity in vitro[J/OL]. Chemistry (Weinheim an Der Bergstrasse, Germany), 2009, 15(45): 12283-12291. DOI:10.1002/chem.200901939.

[122] NIVOROZHKIN A L, SUKHOLENKO E V, NIVOROZHKIN L E, 等. The NMR study of inversion at the metal centre and ligand exchange processes of HgII bis-chelates: X-ray crystal structure of [pyr(NC6H11-c)S]2Hg[J/OL]. Polyhedron, 1989, 8(5): 569-575. DOI:10.1016/S0277-5387(00)83817-6.

[123] ALLISON M, CARAMÉS-MÉNDEZ P, HOFMANN B J, 等. Cytotoxicity of Ruthenium(II) Arene Complexes Containing Functionalized Ferrocenyl β-Diketonate Ligands[J/OL]. Organometallics, 2023, 42(15): 1869-1881. DOI:10.1021/acs.organomet.2c00553.

[124] SHROOT S, PRIOR T J, WILES C, 等. Tethered ruthenium(II) η6-arene complexes: assessing the potential of benzylic substituents to control metal-centred chirality, and applications in asymmetric transfer hydrogenations of ketones[J/OL]. Journal of Organometallic Chemistry, 2022, 960: 122232. DOI:10.1016/j.jorganchem.2021.122232.

[125] MARTÍNEZ-ESTÉVEZ M, GARCÍA-FONTÁN S, ARGIBAY-OTERO S, 等. Synthesis, Characterization, and Cytotoxicity Studies of N-(4-Methoxybenzyl) Thiosemicarbazone Derivatives and Their Ruthenium(II)-p-cymene Complexes[J/OL]. Molecules, 2022, 27(22): 7976. DOI:10.3390/molecules27227976.

7. Abbreviations

°C	degree Celsius
%	percent
µL	microliter
arom.	aromatic
ATP	adenosine triphosphate
Bpin	pinacolborane
brine	saturated sodium chloride solution in water
cat.	catalytic
$CDCl_3$	deuterated chloroform
CH	tertiary carbon
CH_2	secondary carbon
CH_3	primary carbon
Cq	quaternary carbon
d	doublet
dd	doublet of doublets
DCM	dichloromethane
DMSO	dimethyl sulfoxide
DNA	deoxyribonucleic acid
e.g.	exempli gratia
EGFR	external growth factor receptor
EtOAc	ethyl acetate
eq.	equivalent
ER	endoplasmic reticulum
FDA	food and drug administration
g	gram
h	hours
HCl	hydrochloric acid
hept.	heptet
Hz	hertz
J	coupling constant
M	molarity (mol/L)
m	multiplet
MeOD	deuterated methanol
MeOH	methanol

mg	milligram
MHz	megahertz
min	minutes
mL	milliliter
mM	millimolar
mmol	millimol
MTT	3-(4,5-dimethyl-2-thiazolyl)-2,5-diphenyl-2H-tetrazolium bromide
NaOMe	sodium methoxide
NEt_3	triethylamine
NMR	nuclear magnetic resonance
Pd	palladium
ppm	parts per million
r.t.	room temperature
RCHO	aldehyde
Rf	retardation factor
ROS	reactive oxygen species
Ru	ruthenium
s	singlet
t	triplet
tert	tertiary
TLC	thin layer chromatography
VEGF	vascular endothelial growth factor
WHO	world health organisation